

DISCONTINUOUS GALERKIN METHODS FOR THE ACOUSTIC VIBRATION PROBLEM*

FELIPE LEPE[†], DAVID MORA[‡], AND JESUS VELLOJIN[§]

Abstract. In two and three dimension we analyze discontinuous Galerkin methods for the acoustic problem. The acoustic fluid that we consider on this paper is inviscid, leading to a linear eigenvalue problem. The acoustic problem is written, in first place, in terms of the displacement. Under the approach of the non-compact operators theory, we prove convergence and error estimates for the method when the displacement formulation is considered. We analyze the influence of the stabilization parameter on the computation of the spectrum, where spurious eigenmodes arise when this parameter is not correctly chosen. Alternatively we present the formulation depending only on the pressure, comparing the performance of the DG methods with the pure displacement formulation. Computationally, we study the influence of the stabilization parameter on the arising of spurious eigenvalues when the spectrum is computed. Also, we report tests in two and three dimensions where convergence rates are reported, together with a comparison between the displacement and pressure formulations for the proposed DG methods.

1. Introduction. In this paper we are interested in the analysis of a discontinuous Galerkin method (DG) to approximate the natural frequencies of the acoustic problem. The method is based in a interior penalization strategy, in which we focus our attention since the aforementioned parameter may introduce spurious eigenvalues on the computed spectrum.

The DG discretization for eigenvalues is a ongoing research topic where the pioneer work related to this subject is [1], where under suitable norms that depend on jumps and averages, the authors proved spectral correctness and convergence of the DG method for the Laplace eigenvalue problem for both, the primal and mixed formulations. Also, this paper consider symmetric and nonsymmetric DG methods. This study inspired a number of works where DG methods have been considered for other spectral problems [8, 9, 10, 19, 20].

The contribution of the present work is the development of DG methods for the acoustic problem. This problem is one of the most important on engineering and physics, since the correct knowledge of some acoustic fluids, allows to design different structures as containers, motors, vehicles, aircrafts, etc., or noise reduction devices, necessary on the industry. These applications have motivated the development of different numerical methods and approaches such as those of [4, 7, 6, 14, 4, 26, 25, 17]. Some specific applications that deserve to be mentioned are those related to space programs, where mechanical effects of shock, acceleration, and acoustic vibrations are taken into account on the design of durable structures [24]. Also, there is the ultrasonic welding, where ultrasonic acoustic vibrations are used to generate heat and

*Submitted to the editors DATE.

Funding: The first author was partially supported by DIUBB through project 2120173 GI/C Universidad del Bío-Bío and by ANID-Chile through FONDECYT project 11200529 (Chile). The second author was partially supported by DIUBB through project 2120173 GI/C Universidad del Bío-Bío and project Centro de Modelamiento Matemático (CMM), FB210005, BASAL funds for centers of excellence. The second and third author were partially supported by ANID-Chile through project Anillo of Computational Mathematics for Desalination Processes ACT210087.

[†]GIMNAP-Departamento de Matemática, Universidad del Bío - Bío, Casilla 5-C, Concepción, Chile. flepe@ubiobio.cl

[‡]GIMNAP-Departamento de Matemática, Universidad del Bío - Bío, Casilla 5-C, Concepción, Chile and CI²MA, Universidad de Concepción, Chile. dmora@ubiobio.cl

[§]GIMNAP-Departamento de Matemática, Universidad del Bío - Bío, Casilla 5-C, Concepción, Chile. jvellojin@ubiobio.cl

pressure to weld two work pieces together [15]. Another use is found in the acoustic emission detectors, which deals with leaking on pipelines by using the energy signal produced by acoustic vibrations when the fluid escapes [3].

In particular, we are interested in the interior penalization discontinuous Galerkin method (IPDG) in order to obtain a suitable alternative to approximate accurately the eigenfunctions and eigenvalues of the acoustic vibration problem. In recent years, the IPDG has been applied to different eigenvalue problems as for instance, the Maxwell spectral problem [9, 8], the Stokes eigenvalue problem [20], or the elasticity eigenvalue problem [19], where the accuracy on the approximation of the spectrum is remarkable. The IPDG method results to be easy to handle from the computational point of view. This allows the consideration of arbitrary polynomial degrees in two dimensional (resp. three dimensional) convex (resp. non-convex) domain, together with single or mixed boundary conditions. However, the main drawback of the IPDG methods for eigenvalue problems is the correct choice of the penalization parameter, since an incorrect selection of the parameter may introduce spurious eigenvalues. This is an inherent concern that comes with numerical methods that depend on some stabilizations, as for instance the virtual element method (VEM), where in [4, 23, 21], the authors show in their numerical tests that spurious eigenvalues arise when the stabilization parameter changes. The same is observed with IPDG methods such as those of [18, 20], where an analysis of spurious eigenvalues is performed. This is important to take into account, since in real applications, the correct frequencies must be well approximated to avoid undesirable physical phenomena, as for instance, the resonance of certain structures, or the incorrect development of noise insulators.

The available literature for IPDG methods for eigenvalue problems indicates that the correct choice of the aforementioned stabilization parameters depend strongly on the configuration of the problem of interest. This implies that, as the development of the theoretical well posedness of the problem is analyzed, the domain, physical parameters and boundary conditions, need to be taken into account. Also, the polynomial degree for the approximation plays an important role when the stabilization is chosen, since when the polynomial approximation increases, the pollution of the spectrum vanishes, as the computational results available on, for instance, [18, 20] suggests.

With these considerations at hand, our aim is to prove that a IPDG approach is a suitable technique to approximate the natural frequencies of the acoustic eigenvalue problem, where the numerical method, whether symmetric or nonsymmetric, approximates accurately the spectrum, and the stabilization parameter can be chosen with no major problems, according to the needs of the problem. In this sense, we will apply our IPDG methods for the two classic formulations of the acoustic problem: the displacement and pressure formulations, in order to compare the performance of the discontinuous numerical schemes when different unknowns are considered in the mathematical formulation.

The paper is organized as follows: in Section 2, we present the acoustic eigenvalue problem, the displacement formulation and summarize some important results such as the solution operator, regularity properties and the corresponding spectral characterization. Section 3 contains the development of the DG methods, presenting definitions associated to the mesh elements, norms and technical results that are needed for the analysis. Also, we introduce the DG discretization for the acoustic problem and the discrete solution operator that will approximate the continuous one. Also, the spectral analysis is presented, where approximation results and error estimates for the eigenvalues and eigenfunctions are presented. In Section 4 we introduce

the pressure formulation and its DG discretizations, which also are symmetric and nonsymmetric. Finally, in Section 5, we perform a number of numerical tests in two and three dimensions where we analyze, in one hand, the influence of the stabilization parameters on the computation of the spectrum, performing a spurious analysis and, on the other hand, computation of orders of convergence for the eigenvalues. In this section we also compare the performance of the displacement and pressure DG formulations with a benchmark test, where the computational cost is measured through the cpu-time, sparsity and problem size.

1.1. Notations. Throughout this work, Ω is a generic Lipschitz bounded domain of \mathbb{R}^d , where $d \in \{2, 3\}$. For $s \geq 0$, $\|\cdot\|_{s,\Omega}$ stands indistinctly for the norm of the Hilbertian Sobolev spaces $H^s(\Omega)$ or $H^s(\Omega)^d$ with the convention $H^0(\Omega) := L^2(\Omega)$. If X and Y are normed vector spaces, we write $X \hookrightarrow Y$ to denote that X is continuously embedded in Y . We denote by X' and $\|\cdot\|_X$ the dual and the norm of X , respectively. Finally, we employ $\mathbf{0}$ to denote a generic null vector and the relation $\mathbf{a} \lesssim \mathbf{b}$ indicates that $\mathbf{a} \leq C\mathbf{b}$, with a positive constant C which is independent of \mathbf{a} , \mathbf{b} , and the size of the elements in the mesh. The value of C might change at each occurrence. We remark that we will write the constant C only when is needed.

2. The model problem. The acoustic problem reads as follows: Find $\omega \in \mathbb{R}$, the displacement \mathbf{u} and the pressure p on a domain $\Omega \subset \mathbb{R}^d$, such that

$$(2.1) \quad \begin{cases} \nabla p - \omega^2 \rho(x) \mathbf{u} &= \mathbf{0} & \text{in } \Omega \\ p + \rho(x) c^2 \operatorname{div} \mathbf{u} &= 0 & \text{in } \Omega \\ \mathbf{u} \cdot \mathbf{n} &= 0 & \text{on } \partial\Omega, \end{cases}$$

where $\rho(x)$ is the density defined in $x \in \Omega$, c is the sound speed and \mathbf{n} is the outward unitary vector. As an assumption on the density, we consider two constants $\bar{\rho}$ and $\underline{\rho}$, both positives, such that, $\underline{\rho} \leq \rho(x) \leq \bar{\rho}$, for $x \in \Omega$.

Let us introduce the displacement formulation for (2.1). Let us define the space

$$\mathcal{V} := \{\mathbf{v} \in H(\operatorname{div}, \Omega) : \mathbf{v} \cdot \mathbf{n} = 0 \text{ on } \partial\Omega\}.$$

With this space at hand, a variational formulation for the acoustic problem is the following: Find $(\omega, \mathbf{u}) \in \mathbb{R} \times \mathcal{V}$, with $\mathbf{u} \neq \mathbf{0}$, such that

$$(2.2) \quad \int_{\Omega} \rho(x) c^2 \operatorname{div} \mathbf{u} \operatorname{div} \mathbf{v} = \omega^2 \int_{\Omega} \rho(x) \mathbf{u} \cdot \mathbf{v} \quad \forall \mathbf{v} \in \mathcal{V}.$$

Defining $\hat{\lambda} := \omega^2$, we immediately deduce that the eigenspace associated to $\hat{\lambda} = 0$ is

$$\mathcal{K} := \{\mathbf{v} \in \mathcal{V} : \operatorname{div} \mathbf{v} = 0 \text{ in } \Omega\}.$$

We observe that (2.2) is not an elliptic problem. Hence, with a shift argument we obtain the following problem: Find $(\lambda, \mathbf{u}) \in \mathbb{R} \times \mathcal{V}$, with $\mathbf{u} \neq \mathbf{0}$, such that

$$\int_{\Omega} \rho(x) c^2 \operatorname{div} \mathbf{u} \operatorname{div} \mathbf{v} + \int_{\Omega} \rho(x) \mathbf{u} \cdot \mathbf{v} = \lambda \int_{\Omega} \rho(x) \mathbf{u} \cdot \mathbf{v} \quad \forall \mathbf{v} \in \mathcal{V},$$

where $\lambda := 1 + \hat{\lambda}$.

Let us introduce the bilinear forms $a : \mathcal{V} \times \mathcal{V} \rightarrow \mathbb{R}$ and $b : \mathcal{V} \times \mathcal{V} \rightarrow \mathbb{R}$ defined by

$$a(\mathbf{v}, \mathbf{w}) := \int_{\Omega} \rho(x) c^2 \operatorname{div} \mathbf{v} \operatorname{div} \mathbf{w} + \int_{\Omega} \rho(x) \mathbf{v} \cdot \mathbf{w} \quad \forall \mathbf{v}, \mathbf{w} \in \mathcal{V}.$$

and

$$b(\mathbf{v}, \mathbf{w}) := \int_{\Omega} \rho(x) \mathbf{v} \cdot \mathbf{w}, \quad \forall \mathbf{v}, \mathbf{w} \in \mathcal{V}.$$

With these bilinear forms at hand, problem (2.2) is rewritten as follows: Find $(\lambda, \mathbf{u}) \in \mathbb{R} \times \mathcal{V}$, with $\mathbf{u} \neq \mathbf{0}$, such that

$$(2.3) \quad a(\mathbf{u}, \mathbf{v}) = \lambda b(\mathbf{u}, \mathbf{v}) \quad \forall \mathbf{v} \in \mathcal{V}.$$

Clearly $a(\cdot, \cdot)$ is continuous, in the sense that there exists a positive constant $M := \|\rho\|_{\infty, \Omega} \min\{c^2, 1\}$ such that $|a(\mathbf{u}, \mathbf{v})| \leq M \|\mathbf{u}\|_{\text{div}, \Omega} \|\mathbf{v}\|_{\text{div}, \Omega}$. Observe that for any $\mathbf{v} \in \mathcal{V}$ there holds

$$(2.4) \quad a(\mathbf{v}, \mathbf{v}) \geq \underline{\rho} c^2 \|\text{div } \mathbf{v}\|_{0, \Omega}^2 + \underline{\rho} \|\mathbf{v}\|_{0, \Omega}^2 \geq \underbrace{\min\{\underline{\rho} c^2, \underline{\rho}\}}_{\alpha^c} \|\mathbf{v}\|_{\text{div}, \Omega}^2,$$

implying the coercivity of $a(\cdot, \cdot)$ with a constant $\alpha^c := \min\{\underline{\rho} c^2, \underline{\rho}\}$. This allows us to introduce the so called solution operator associated to (2.3), defined by $\mathbf{T} : \mathcal{V} \rightarrow \mathcal{V}$ where for a given $\mathbf{f} \in \mathcal{V}$, we have $\mathbf{T}\mathbf{f} = \hat{\mathbf{u}}$, where $\hat{\mathbf{u}}$ is the solution of the source problem

$$a(\hat{\mathbf{u}}, \mathbf{v}) = b(\mathbf{f}, \mathbf{v}) \quad \forall \mathbf{v} \in \mathcal{V}.$$

Note that operator \mathbf{T} is well defined and bounded thanks to Lax-Milgram's lemma, non-compact, and selfadjoint respect to $a(\cdot, \cdot)$ and $b(\cdot, \cdot)$. Moreover, (λ, \mathbf{u}) is a solution of (2.2) if and only if $(1/\lambda, \mathbf{u})$ is an eigenpair of \mathbf{T} .

Let us remark that since we have the space \mathcal{K} at hand, there exists an operator $\mathbf{P} : \mathcal{V} \rightarrow \mathcal{V}$ such that the space \mathcal{V} can be decomposed as a direct sum given by $\mathcal{V} = \mathcal{K} \oplus \mathbf{P}(\mathcal{V})$, where $\mathbf{P}(\mathcal{V})$ is the orthogonal complement of \mathcal{K} with respect to the inner product defined in \mathcal{V} .

The following technical results is available in [4, 5].

LEMMA 2.1 (Orthogonal complement). *The space $\mathbf{P}(\mathcal{V})$ is defined by $\mathbf{P}(\mathcal{V}) := \{\nabla q : q \in H^1(\Omega)\}$ and satisfies $\mathcal{V} = \mathcal{K} \oplus \mathbf{P}(\mathcal{V})$, which is a orthogonal decomposition in $L^2(\Omega)^d$ and $H(\text{div}, \Omega)$. Moreover, there exists $s \in (1/2, 1]$ such that for all $\mathbf{v} \in \mathcal{V}$, if $\mathbf{v} = \boldsymbol{\varphi} + \nabla q$, with $\boldsymbol{\varphi} \in \mathcal{K}$ and $\nabla q \in \mathbf{P}(\mathcal{V})$, then $\nabla q \in H^s(\Omega)^d$ and $\|\nabla q\|_{s, \Omega} \lesssim \|\text{div } \mathbf{v}\|_{0, \Omega}$.*

Now we recall some important properties that \mathbf{T} satisfies.

LEMMA 2.2 (Invariance of \mathbf{T} on $\mathbf{P}(\mathcal{V})$). *There holds $\mathbf{T}(\mathbf{P}(\mathcal{V})) \subset \mathbf{P}(\mathcal{V})$. Also, there holds*

$$\mathbf{T}(\mathbf{P}(\mathcal{V})) \subset \{\mathbf{v} \in H^s(\Omega)^d : \text{div } \mathbf{v} \in H^1(\Omega)\},$$

and for all $\mathbf{f} \in \mathcal{G} \cap \mathcal{V}$, if $\mathbf{u} = \mathbf{T}\mathbf{f}$, the following estimate holds

$$\|\mathbf{u}\|_{s, \Omega} + \|\text{div } \mathbf{u}\|_{1+s, \Omega} \lesssim \|\mathbf{f}\|_{\text{div}, \Omega},$$

where this estimate is obtained with a bootstrap argument. Moreover, we have that $\mathbf{T}|_{\mathbf{P}(\mathcal{V})} : \mathbf{P}(\mathcal{V}) \rightarrow \mathbf{P}(\mathcal{V})$ is compact.

Finally, we present the following spectral characterization of \mathbf{T} .

THEOREM 2.3. *The spectrum of \mathbf{T} decomposes as $\text{sp}(\mathbf{T}) = \{0, 1\} \cup \{\mu_k\}_{k \in \mathbb{N}}$ where*

1. $\mu = 1$ is an infinite-multiplicity eigenvalue of \mathbf{T} and its associated eigenspace is \mathcal{K} ,

2. $\{\mu_k\}_{k \in \mathbb{N}} \subset (0, 1)$ is a sequence of finite-multiplicity eigenvalues if \mathbf{T} which converge to zero and if \mathbf{u} is an eigenfunction of \mathbf{T} associated with such an eigenvalue, then there exists $\hat{s} > 1/2$, depending on the eigenvalue, such that

$$\|\mathbf{u}\|_{\hat{s}, \Omega} + \|\operatorname{div} \mathbf{u}\|_{1+\hat{s}, \Omega} \lesssim \|\mathbf{u}\|_{\operatorname{div}, \Omega},$$

where the hidden constant also depends on the eigenvalue.

3. $\mu = 0$ is not an eigenvalue of \mathbf{T} .

With this result at hand, we are in a position to introduce the numerical method of our interest.

3. The DG method. To begin, we need to set some definitions and preliminaries. For $\Omega \subset \mathbb{R}^d$, for $d \in \{2, 3\}$, let \mathcal{T}_h be a shape regular family of meshes which subdivide the domain $\bar{\Omega}$ into triangles/tetrahedra K . We denote by h_K the diameter of the element $K \in \mathcal{T}_h$ and h the maximum of the diameters of all the elements of the mesh, i.e. $h := \max_{K \in \mathcal{T}_h} \{h_K\}$. Let F be a closed set such that $F \subset \bar{\Omega}$ is an interior edge/face if F has a positive $(n-1)$ -dimensional measure and if there are distinct elements K and K' such that $F = \bar{K} \cap \bar{K}'$. A closed subset $F \subset \bar{\Omega}$ is a boundary edge/face if there exists $K \in \mathcal{T}_h$ such that F is an edge/face of K and $F = \bar{K} \cap \partial\Omega$. Let \mathcal{F}_h^* and \mathcal{F}_h^∂ be the sets of interior edges/faces and boundary edges/face, respectively.

For any $t \geq 0$, we define the following broken Sobolev space

$$H^t(\mathcal{T}_h)^d := \{\mathbf{v} \in L^2(\Omega)^d : \mathbf{v}|_K \in H^t(K)^d \quad \forall K \in \mathcal{T}_h\}.$$

Also, the space of the skeletons of the triangulations \mathcal{T}_h is defined by $L^2(\mathcal{F}_h) := \prod_{F \in \mathcal{F}_h} L^2(F)$, where $\mathcal{F}_h := \mathcal{F}_h^* \cup \mathcal{F}_h^\partial$.

In the forthcoming analysis, $h_{\mathcal{F}} \in L^2(\mathcal{F}_h)$ will represent the piecewise constant function defined by $h_{\mathcal{F}}|_F := h_F$ for all $F \in \mathcal{F}_h$, where h_F denotes the diameter of edge/face F .

Let $\mathcal{P}_m(\mathcal{T}_h)$ be the space of piecewise polynomials respect with to \mathcal{T}_h of degree at most $m \geq 0$; namely,

$$\mathcal{P}_m(\mathcal{T}_h) := \{v \in L^2(\Omega) : v|_K \in \mathcal{P}_m(K) \quad \forall K \in \mathcal{T}_h\}.$$

For any $k \geq 1$, we define the finite element spaces $\mathcal{V}_h := \mathcal{P}_k(\mathcal{T}_h)^d$ and $\mathcal{V}_h^c := \mathcal{V}_h \cap \mathcal{V}$. We observe that the space \mathcal{V}_h^c is the Brezzi-Douglas-Marini (BDM) finite element space. Now, we recall some well-known properties of the space \mathcal{V}_h^c .

We define averages $\{\mathbf{v}\} \in L^2(\mathcal{F}_h)^d$ and jumps $[\![\mathbf{v}]\!] \in L^2(\mathcal{F}_h)$ as follows

$$\{\mathbf{v}\}_F := (\mathbf{v}_K + \mathbf{v}_{K'})/2 \quad \text{and} \quad [\![\mathbf{v}]\!]_F := \mathbf{v}_K \cdot \mathbf{n}_K + \mathbf{v}_{K'} \cdot \mathbf{n}_{K'} \quad \forall F \in \mathcal{F}(K) \cap \mathcal{F}(K'),$$

where \mathbf{n}_K is the outward unit normal vector to ∂K . Also, on the boundary $\partial\Omega$ and for all $F \in \mathcal{F}(K) \cap \partial\Omega$, the averages and jumps are defined by $\{\mathbf{v}\}_F := \mathbf{v}_K$ and $[\![\mathbf{v}]\!]_F := \mathbf{v}_K \cdot \mathbf{n}$, respectively.

Before concluding this section, we shall note some results required for the analysis that follows. For a vector field $\mathbf{v} \in \mathcal{V}_h$ we define $\operatorname{div}_h \mathbf{v} \in L^2(\Omega)$ by $\operatorname{div}_h \mathbf{v}|_K := \operatorname{div}(\mathbf{v}|_K)$ for all $K \in \mathcal{T}_h$ and we endow $\mathcal{V}(h) := \mathcal{V} + \mathcal{V}_h$ with the following seminorm

$$|\mathbf{v}|_{\mathcal{V}(h)}^2 := \|\operatorname{div}_h \mathbf{v}\|_{0,\Omega}^2 + \|h_{\mathcal{F}}^{-1/2} [\![\mathbf{v}]\!]\|_{0,\mathcal{F}_h^*}^2,$$

which is well defined in $\mathcal{V}(h)$ and the norm $\|\mathbf{v}\|_{\operatorname{DG}}^2 := |\mathbf{v}|_{\mathcal{V}(h)}^2 + \|\mathbf{v}\|_{0,\Omega}^2$. Another important ingredient for the analysis is the following discrete trace inequality [13]:

$$(3.1) \quad \|h^{1/2} \{\mathbf{v}\}\|_{0,\mathcal{F}} \lesssim \|\mathbf{v}\|_{0,\Omega} \quad \forall \mathbf{v} \in \mathcal{P}_k(\mathcal{T}_h).$$

3.1. The DG acoustic problem. Now we introduce the DG discretization for the acoustic problem (2.2), which reads as follows: Find $\lambda_h := 1 + \widehat{\lambda}_h \in \mathbb{C}$ and $\mathbf{0} \neq \mathbf{u}_h \in \mathcal{V}_h$ such that

$$(3.2) \quad a_h(\mathbf{u}_h, \boldsymbol{\tau}_h) = \lambda_h b(\mathbf{u}_h, \boldsymbol{\tau}_h) \quad \forall \boldsymbol{\tau}_h \in \mathcal{V}_h,$$

where the bilinear form $a_h : \mathcal{V}_h \times \mathcal{V}_h \rightarrow \mathbb{C}$ is defined by

$$(3.3) \quad a_h(\mathbf{u}_h, \mathbf{v}_h) := \int_{\Omega} \rho(x) c^2 \operatorname{div}_h \mathbf{u}_h \operatorname{div}_h \mathbf{v}_h + \int_{\Omega} \rho(x) \mathbf{u}_h \cdot \mathbf{v}_h \\ + \int_{\mathcal{F}_h^*} \frac{\mathbf{a}_S}{h_{\mathcal{F}}} \llbracket \mathbf{u}_h \rrbracket \cdot \llbracket \mathbf{v}_h \rrbracket - \int_{\mathcal{F}_h^*} \{\rho(x) c^2 \operatorname{div}_h \mathbf{u}_h\} \cdot \llbracket \mathbf{v}_h \rrbracket - \varepsilon \int_{\mathcal{F}_h^*} \{\rho(x) c^2 \operatorname{div}_h \mathbf{v}_h\} \cdot \llbracket \mathbf{u}_h \rrbracket,$$

where $\mathbf{a}_S > 0$ is the so called stabilization parameter and $\varepsilon \in \{-1, 0, 1\}$. These parameters are relevant for our DG methods. In one hand, the stabilization \mathbf{a}_S is a parameter that, if is not correctly chosen, could yield to instabilities for the method. In general, this parameter depends on theoretical and physical constants and, in the numerical performance, also on the polynomial degrees. (cf. Section 5). On the other hand, ε establishes if the DG method is symmetric or nonsymmetric. More precisely, if $\varepsilon = 1$ we obtain the classic symmetric interior penalty method (SIP), if $\varepsilon = -1$ we obtain the non-symmetric interior penalty method (NIP) and if $\varepsilon = 0$ the incomplete interior penalty method (IIP) (see [1, 20, 19] for instance).

For the analysis, we introduce the following norm

$$\|\mathbf{u}\|_{\text{DG}}^* := \left(\|\mathbf{u}\|_{\text{DG}}^2 + \|h_{\mathcal{F}_h}^{1/2} \{\operatorname{div}_h \mathbf{u}\}\|_{0, \mathcal{F}_h^*}^2 \right)^{1/2}.$$

It is easy to check that for all $\mathbf{u}, \mathbf{v} \in \mathcal{V}(h)$, and $\operatorname{div} \mathbf{u}, \operatorname{div} \mathbf{v} \in H^t(\Omega)$ with $t > 1/2$, the bilinear form $a_h(\cdot, \cdot)$ is bounded. In fact, there exists a constant $C > 0$, independent of h , such that $|a_h(\mathbf{u}, \mathbf{v})| \leq C \|\mathbf{u}\|_{\text{DG}}^* \|\mathbf{v}\|_{\text{DG}}^*$. Moreover, by means of (3.1) it is possible to prove that for all $\mathbf{v}_h \in \mathcal{V}_h$ there exists a positive constant M_{DG} such that $|a_h(\mathbf{u}, \mathbf{v}_h)| \leq M_{\text{DG}} \|\mathbf{u}\|_{\text{DG}}^* \|\mathbf{v}_h\|_{\text{DG}}$.

In order to analyze the discrete eigenvalue problem (3.2), we need to decompose the space \mathcal{V}_h^c . With this aim, we consider the following subspace of \mathcal{K}

$$\mathcal{K}_h := \{\mathbf{v}_h \in \mathcal{V}_h^c : \operatorname{div} \mathbf{v}_h = 0\}.$$

With \mathcal{K}_h at hand, we are interested in its orthogonal complement at the discrete level. With this in mind, is necessary to introduce the discrete counterpart of the operator \mathbf{P} , which we denote by \mathbf{P}_h and is defined by $\mathbf{P}_h : \mathcal{V}_h^c \rightarrow \mathcal{V}_h^c$. With this operator at hand, the following approximation result holds, and its proof is identical to [20, Lemma 3.1].

LEMMA 3.1. *The operator $\mathbf{P}_h : \mathcal{V}_h^c \rightarrow \mathcal{V}_h^c$ is a projection with kernel \mathcal{K}_h and satisfies the following estimate*

$$\|(\mathbf{P} - \mathbf{P}_h)\mathbf{v}_h\|_{\operatorname{div}, \Omega} \lesssim h^s \|\operatorname{div} \mathbf{v}_h\|_{0, \Omega} \quad \forall \mathbf{v}_h \in \mathcal{V}_h^c,$$

where the hidden constant is independent of h and s is as in Lemma 2.1.

The following technical result proved in [22, Proposition 5.2] for tensorial fields, and that is easily adapted for vectorial fields, will be useful in the forthcoming analysis.

PROPOSITION 3.2. *There exist a projection $\mathcal{I}_h : \mathcal{V}_h \rightarrow \mathcal{V}_h^c$ and two constants $\underline{C}, \bar{C} > 0$, independent of h , such that*

$$(3.4) \quad \underline{C} \|\mathbf{v}_h\|_{\text{DG}} \leq \left(\|\mathcal{I}_h \mathbf{v}_h\|_{\text{div}, \Omega}^2 + \|h_{\mathcal{F}}^{-1/2} \llbracket \mathbf{v}_h \rrbracket \|_{0, \mathcal{F}_h^*}^2 \right)^{1/2} \leq \bar{C} \|\mathbf{v}_h\|_{\text{DG}} \quad \forall \mathbf{v}_h \in \mathcal{V}_h.$$

Moreover, we have that

$$(3.5) \quad \|\text{div}_h(\mathbf{v}_h - \mathcal{I}_h \mathbf{v}_h)\|_{0, \Omega}^2 + \sum_{K \in \mathcal{T}_h} h_K^{-2} \|\mathbf{v}_h - \mathcal{I}_h \mathbf{v}_h\|_{0, K}^2 \leq C \|h_{\mathcal{F}}^{-1/2} \llbracket \mathbf{v}_h \rrbracket \|_{0, \mathcal{F}_h^*}^2,$$

with $C > 0$ independent of h .

Now, with this result at hand, we will prove that $a_h(\cdot, \cdot)$ is coercive in \mathcal{V}_h , independent of the DG method that we are considering.

LEMMA 3.3. *For any $\varepsilon \in \{-1, 0, 1\}$, there exists a parameter $\mathbf{a}^* > 0$ such that for all $\mathbf{a}_S \geq \mathbf{a}^*$ there holds*

$$a_h(\mathbf{v}_h, \mathbf{v}_h) \geq \alpha_{\text{DG}} \|\mathbf{v}_h\|_{\text{DG}}^2 \quad \forall \mathbf{v}_h \in \mathcal{V}_h,$$

where $\alpha_{\text{DG}} > 0$ is independent of h .

Proof. The proof follows the same arguments of those in [20, Lemma 3.2], taking into account for our case, the presence of density and sound speed of the fluid. \square

REMARK 3.1. *Notice that the coercivity constant of $a_h(\cdot, \cdot)$ depends strongly on the physical parameters, namely the density and sound speed. Hence, the stability of the method will depend on the configuration of the problem where these parameters play an important role, together with the geometry of domain, since the constants that appear on the discrete trace inequality (3.1) and Proposition 3.2 depend on Ω . This is important to have in mind, since as we will analyze in the numerical section (cf. Section 5), the appearance of spurious modes depend on the choice of \mathbf{a} and hence, on \mathbf{a}^* .*

We notice that the discrete coercivity of $a_h(\cdot, \cdot)$ holds true for any $\varepsilon \in \{-1, 0, 1\}$. Implying that symmetric and nonsymmetric methods are well posed with our DG approach. Moreover, we introduce the discrete solution operator associated to (3.2):

$$\mathbf{T}_h^\varepsilon : \mathcal{V} \rightarrow \mathcal{V}_h, \quad \mathbf{f} \mapsto \mathbf{T}_h^\varepsilon \mathbf{f} := \tilde{\mathbf{u}}_h^\varepsilon,$$

where $\tilde{\mathbf{u}}_h^\varepsilon \in \mathcal{V}_h$ is the unique solution of the following discrete source problem:

$$a_h(\tilde{\mathbf{u}}_h^\varepsilon, \mathbf{v}_h) = b(\mathbf{f}, \mathbf{v}_h) \quad \forall \mathbf{v}_h \in \mathcal{V}_h.$$

Observe that the superindex ε denotes if the operator is associated to a symmetric or nonsymmetric method. This is important to have in mind since the choice of ε leads to different solutions that lie on real or complex spaces.

Clearly \mathbf{T}_h^ε is well defined thanks to Lax-Milgram's lemma. Moreover, there exists a constant $C > 0$ independent of h such that $\|\mathbf{T}_h^\varepsilon \mathbf{f}\|_{\text{DG}} \leq C \|\mathbf{f}\|_{\text{div}, \Omega}$, for all $\mathbf{f} \in \mathcal{V}$. Also, It is easy to check that $(\lambda_h, \mathbf{u}_h) \in \mathbb{C} \times \mathcal{V}_h$ is a solution of problem (3.2) if and only if $(\mu_h, \mathbf{u}_h) \in \mathbb{C} \times \mathcal{V}_h$ with $\mu_h = 1/\lambda_h$ is an eigenpair of \mathbf{T}_h^ε , i.e., $\mathbf{T}_h^\varepsilon \mathbf{u}_h = \frac{1}{\mu_h} \mathbf{u}_h$.

PROPOSITION 3.4. *Let $\mathbf{f} \in \mathbf{P}(\mathcal{V})$ be such that $\mathbf{T} \mathbf{f} := \tilde{\mathbf{u}}$. Then, for any $\varepsilon \in \{-1, 0, 1\}$ the following best approximation result holds*

$$\|(\mathbf{T} - \mathbf{T}_h^\varepsilon) \mathbf{f}\|_{\text{DG}} \leq \frac{M_{\text{DG}}}{\alpha_{\text{DG}}} \inf_{\mathbf{v}_h \in \mathcal{V}_h} \|\mathbf{T} \mathbf{f} - \mathbf{v}_h\|_{\text{DG}}^*.$$

Moreover, for s as in Lemma 2.1, the following estimate holds

$$\|(\mathbf{T} - \mathbf{T}_h^\varepsilon)\mathbf{f}\|_{\text{DG}} \lesssim h^s (\|\tilde{\mathbf{u}}\|_{s,\Omega} + \|\operatorname{div} \tilde{\mathbf{u}}\|_{1+s,\Omega}),$$

where the hidden constant is independent of h .

Finally we derive the following result which holds for symmetric and non symmetric methods.

LEMMA 3.5. *For any $\mathbf{v}_h \in \mathcal{V}_h$, the following estimate holds*

$$\|(\mathbf{T} - \mathbf{T}_h^\varepsilon)\mathbf{v}_h\|_{\text{DG}} \lesssim h^s \|\mathbf{v}_h\|_{\text{DG}},$$

where s is the exponent provided by Lemma 2.1

3.2. Convergence analysis and error estimates. Since the solution operator \mathbf{T} is non compact, the analysis of the spectral convergence and error estimates will be performed under the approach of the theory of [11, 12]. Let us recall the following definitions, needed to perform the analysis.

- P1. $\|\mathbf{T} - \mathbf{T}_h^\varepsilon\|_{\mathcal{L}(\mathcal{V}_h, \mathcal{V}(h))} \rightarrow 0$ as $h \rightarrow 0$.
- P2. $\forall \mathbf{v} \in \mathcal{V}$, there holds

$$\inf_{\mathbf{v}_h \in \mathcal{V}_h} \|\mathbf{v} - \mathbf{v}_h\|_{\text{DG}} \rightarrow 0 \quad \text{as } h \rightarrow 0.$$

In order to prove convergence between eigenspaces, we introduce the following definitions: let $\mathbf{x} \in \mathcal{V}(h)$ and \mathbb{E} and \mathbb{F} be closed subspaces of $\mathcal{V}(h)$. We define

$$\delta(\mathbf{x}, \mathbb{E}) := \inf_{\mathbf{y} \in \mathbb{E}} \|\mathbf{x} - \mathbf{y}\|_{\text{DG}}, \quad \delta(\mathbb{E}, \mathbb{F}) := \sup_{\mathbf{y} \in \mathbb{E}: \|\mathbf{y}\|_{\text{DG}}=1} \delta(\mathbf{y}, \mathbb{F}).$$

Hence, the gap between two closed subspaces is defined by

$$\widehat{\delta}(\mathbb{E}, \mathbb{F}) := \max\{\delta(\mathbb{E}, \mathbb{F}), \delta(\mathbb{F}, \mathbb{E})\}.$$

Let $\lambda \in (0, 1)$ be an isolated eigenvalue of \mathbf{T} and let D an open disk in the complex plane with boundary γ such that λ is the only eigenvalue of \mathbf{T} lying in D and $\gamma \cap \operatorname{sp}(\mathbf{T}) = \emptyset$. We introduce the spectral projector corresponding to the continuous and discrete solution operators \mathbf{T} and \mathbf{T}_h^ε , respectively

$$\begin{aligned} \mathcal{E} &:= \frac{1}{2\pi i} \int_{\gamma} (z\mathbf{I} - \mathbf{T})^{-1} dz : \mathcal{V}(h) \longrightarrow \mathcal{V}(h), \\ \mathcal{E}_h &:= \frac{1}{2\pi i} \int_{\gamma} (z\mathbf{I} - \mathbf{T}_h^\varepsilon)^{-1} dz : \mathcal{V}(h) \longrightarrow \mathcal{V}(h) \end{aligned}$$

where \mathcal{E}_h is well-defined and bounded uniformly in h . Moreover, $\mathcal{E}|_{\mathcal{V}}$ is a spectral projection in \mathcal{V} onto the (finite dimensional) eigenspace $\mathcal{E}(\mathcal{V})$ corresponding to the eigenvalue λ of \mathbf{T} . In fact, we have that $\mathcal{E}(\mathcal{V}(h)) = \mathcal{E}(\mathcal{V})$ (see [19] for further details). Moreover, $\mathcal{E}_h|_{\mathcal{V}_h}$ is a projector in \mathcal{V}_h onto the eigenspace $\mathcal{E}_h(\mathcal{V}_h)$ corresponding to the eigenvalues of $\mathbf{T}_h^\varepsilon : \mathcal{V}_h \rightarrow \mathcal{V}_h$ contained in γ . We also have that $\mathcal{E}_h(\mathcal{V}(h)) = \mathcal{E}_h(\mathcal{V}_h)$.

Now, we will compare $\mathcal{E}_h(\mathcal{V}_h)$ to $\mathcal{E}(\mathcal{V})$ in terms of the gap $\widehat{\delta}$. The proof of the next auxiliary result follows from the definition of \mathcal{E} and \mathcal{E}_h .

LEMMA 3.6. *The following estimate holds*

$$\|\mathcal{E} - \mathcal{E}_h\|_{\mathcal{L}(\mathcal{V}_h, \mathcal{V}(h))} \leq C \|\mathbf{T} - \mathbf{T}_h^\varepsilon\|_{\mathcal{L}(\mathcal{V}_h, \mathcal{V}(h))},$$

where the hidden constant is independent of h .

The following result will be used to establish the approximation properties of the eigenfunctions of the continuous problem by means of those of the discrete DG discretization (see [20, Lemma 4.5]).

LEMMA 3.7. *The following estimate holds*

$$\widehat{\delta}(\mathcal{E}(\mathcal{V}), \mathcal{E}_h(\mathcal{V}_h)) \leq C \left(\|\mathbf{T} - \mathbf{T}_h^\varepsilon\|_{\mathcal{L}(\mathcal{V}_h, \mathcal{V}(h))} + \delta(\mathcal{E}(\mathcal{V}), \mathcal{V}_h) \right),$$

where the hidden constant is independent of h .

Now, we state the convergence properties of the DG methods.

THEOREM 3.8. *Let $\lambda \in (0, 1)$ be an eigenvalue of \mathbf{T} of algebraic multiplicity m and let D_λ be a closed disk in the complex plane centered at κ with boundary γ such that $D_\lambda \cap \text{sp}(\mathbf{T}) = \{\kappa\}$. Let $\lambda_{1,h}, \dots, \lambda_{m(h),h}$ be the eigenvalues of \mathbf{T}_h^ε lying in D_λ and repeated according to their algebraic multiplicity. Then, for any DG method defined by $\varepsilon \in \{-1, 0, 1\}$, we have that $m(h) = m$ for h sufficiently small and*

$$\lim_{h \rightarrow 0} \max_{1 \leq i \leq m} |\lambda - \lambda_{i,h}| = 0.$$

Moreover, if $\mathcal{E}(\mathcal{V})$ is the eigenspace corresponding to λ and $\mathcal{E}_h(\mathcal{V}_h)$ is the \mathbf{T}_h^ε -invariant subspace of \mathcal{V}_h spanned by the eigenspaces corresponding to $\{\lambda_{i,h}, i = 1, \dots, m\}$ then

$$\lim_{h \rightarrow 0} \widehat{\delta}(\mathcal{E}(\mathcal{V}), \mathcal{E}_h(\mathcal{V}_h)) = 0.$$

Proof. See proof of [19, Theorem 5.2]. □

Let us introduce the following distance

$$\delta^*(\mathcal{E}(\mathcal{V}), \mathcal{V}_h) := \sup_{\substack{\mathbf{v} \in \mathcal{E}(\mathcal{V}) \\ \|\mathbf{v}\|_{\text{DG}}=1}} \inf_{\mathbf{v}_h \in \mathcal{V}_h} \|\mathbf{v} - \mathbf{v}_h\|_{\text{DG}}^*.$$

With this distance at hand, we derive the following results, which have been established in [19, Theorem 6.1] for a fixed eigenvalue $\lambda \in (0, 1)$ of \mathbf{T} .

THEOREM 3.9. *For h small enough, the following estimate holds*

$$\widehat{\delta}(\mathcal{E}(\mathcal{V}), \mathcal{E}_h(\mathcal{V}_h)) \lesssim \delta^*(\mathcal{E}(\mathcal{V}), \mathcal{V}_h),$$

where the hidden constant is independent of h .

Finally, with the aid of Proposition 2.1, we present the rates of convergence of the proposed DG methods. The proof of the following result is identical to the one contained in [20, Theorem 4.4] and holds for both, symmetric and nonsymmetric DG methods.

THEOREM 3.10. *Let $r > 0$ be such that $\mathcal{E}(\mathcal{V}) \subset \{\mathbf{v} \in \mathbf{H}^r(\Omega) : \text{div } \mathbf{v} \in \mathbf{H}^{1+r}(\Omega)^n\}$ (cf. Proposition 2.1). Then, for $\varepsilon \in \{-1, 0, 1\}$ we have*

$$\widehat{\delta}(\mathcal{E}_h(\mathcal{V}_h), \mathcal{E}(\mathcal{V})) \lesssim h^{\min\{r,k\}} \quad \text{and} \quad \max_{1 \leq i \leq m} |\lambda - \lambda_{i,h}| \lesssim h^{\sigma \min\{r,k\}},$$

where $\sigma := \frac{(\varepsilon+2)^\varepsilon - 1}{2} + 1$ and the hidden constants are independent of h .

4. The pressure formulation. An alternative approach to analyze the acoustic problem (2.1) is to consider the pressure formulation which is obtained eliminating the displacement in (2.1), using the second equation, in order to write

$$(4.1) \quad \begin{cases} c^2 \operatorname{div} \left(\frac{1}{\rho(x)} \nabla p \right) + \frac{\omega^2}{\rho(x)} p = 0 & \text{in } \Omega, \\ \frac{\partial p}{\partial \mathbf{n}} = 0 & \text{on } \partial\Omega, \end{cases}$$

where (4.1) is now a scalar problem. Clearly the displacement is recovered with a postprocess of the pressure, using the first equation on (2.1). Let us remark that the computed solutions, namely the eigenvalues and eigenfunctions, are exactly the same when the pure displacement formulation is considered. A variational formulation for this problem is: Find $\omega \in \mathbb{R}$ and $0 \neq p \in H^1(\Omega)$ such that

$$\int_{\Omega} \frac{1}{\rho(x)} \nabla p \cdot \nabla v = \omega^2 \int_{\Omega} \frac{1}{\rho(x)} p v \quad \forall v \in H^1(\Omega).$$

With a shift argument we arrive to the following problem: Find $\omega \in \mathbb{R}$ and $0 \neq p \in H^1(\Omega)$ such that

$$(4.2) \quad a^p(p, v) = (\omega^2 + 1) b^p(p, v) \quad \forall v \in H^1(\Omega),$$

where the bilinear forms $a : H^1(\Omega) \times H^1(\Omega) \rightarrow \mathbb{R}$ and $b : H^1(\Omega) \times H^1(\Omega) \rightarrow \mathbb{R}$ are defined for all $q, v \in H^1(\Omega)$ by

$$a^p(q, v) := c^2 \int_{\Omega} \frac{1}{\rho(x)} \nabla q \cdot \nabla v + \int_{\Omega} \frac{1}{\rho(x)} q v \quad \text{and} \quad b^p(q, v) := \int_{\Omega} \frac{1}{\rho(x)} q v.$$

Note that $a^p(\cdot, \cdot)$ is coercive in $H^1(\Omega)$. Also, the solution operator $T^p : L^2(\Omega) \rightarrow H^1(\Omega) \hookrightarrow L^2(\Omega)$ is defined by $T^p f = \tilde{p}$ where $\tilde{p} \in H^1(\Omega)$ is the solution of the corresponding associated source problem. This solution operator results to be compact due the compact inclusion of $H^1(\Omega)$ onto $L^2(\Omega)$. On the other hand, from Lemma 2.2, we have that $\mathbf{u} \in H^s(\Omega)$ with $s \in (1/2, 1]$. Hence, from the first equation of (2.1) we have that $\nabla p \in H^s(\Omega)$ and hence $p \in H^{1+s}(\Omega)$, providing the regularity requirement for the eigenfunctions when problem (4.2) is considered. For this case, and for any $k \geq 1$, the finite element spaces are $\mathcal{V}_h^p := \mathcal{P}_k(\mathcal{T}_h)$ and $\mathcal{V}_h^{p,c} := \mathcal{V}_h^p \cap H^1(\Omega)$, which now are scalar. Inspired by the analysis of [1], let us define $\mathcal{V}^p(h) := H^1(\Omega) + \mathcal{V}_h^p$ which we endow with the following seminorm $\|v\|_{\mathcal{V}(h)}^2 = \|\nabla_h v\|_{0,\Omega}^2 + \|h_{\mathcal{F}}^{-1/2} \llbracket v \rrbracket\|_{0,\mathcal{F}_h}^2$. Then, we define the norm $\|v_h\|_{DG}^2 = \|v_h\|_{0,\Omega}^2 + \|v_h\|_{\mathcal{V}(h)}^2$.

The DG discretization for problem (4.2) is as follows: Find $\omega_h \in \mathbb{C}$ and $0 \neq p_h \in \mathcal{V}_h^p$ such that

$$(4.3) \quad a_h^p(p_h, v_h) = (\omega_h^2 + 1) b_h^p(p_h, v_h) \quad \forall v_h \in \mathcal{V}_h^p,$$

where

$$\begin{aligned} a_h^p(p_h, v_h) := & c^2 \int_{\Omega} \frac{1}{\rho(x)} \nabla_h p_h \cdot \nabla_h v_h + \int_{\Omega} \frac{1}{\rho(x)} p_h v_h + \int_{\mathcal{F}_h^*} \frac{\mathbf{a}_{S,p}}{h_{\mathcal{F}}} \llbracket p_h \rrbracket \cdot \llbracket v_h \rrbracket \\ & - \int_{\mathcal{F}_h^*} \frac{1}{\rho(x)} \{c^2 \nabla_h p_h\} \cdot \llbracket v_h \rrbracket - \varepsilon \int_{\mathcal{F}_h^*} \frac{1}{\rho(x)} \{c^2 \nabla_h v_h\} \cdot \llbracket p_h \rrbracket. \end{aligned}$$

Let us prove that $a_h^p(\cdot, \cdot)$ is coercive in \mathcal{V}_h^p .

LEMMA 4.1 (ellipticity of $a_h^p(\cdot, \cdot)$). *For any $\varepsilon \in \{-1, 0, 1\}$, there exists a positive parameter \mathbf{a}_p^* such that for all $\mathbf{a}_{S,p} \geq \mathbf{a}_p^*$ there holds*

$$a_h^p(v_h, v_h) \geq \alpha_p \|v_h\|_{DG}^2 \quad \forall v_h \in \mathcal{V}_h^p,$$

where $\alpha_p > 0$ is independent of h .

Proof. Let $v_h \in \mathcal{V}_h^p$. Then, from the definition of $a_h^p(\cdot, \cdot)$ we have

$$\begin{aligned} a_h^p(v_h, v_h) &= c^2 \int_{\Omega} \frac{1}{\rho(x)} \nabla_h v_h \cdot \nabla_h v_h + \int_{\Omega} \frac{1}{\rho(x)} v_h v_h + \int_{\mathcal{F}_h^*} \frac{\mathbf{a}_{S,p}}{h_{\mathcal{F}}} \llbracket v_h \rrbracket \cdot \llbracket v_h \rrbracket \\ &\quad - \int_{\mathcal{F}_h^*} \frac{1}{\rho(x)} \{c^2 \nabla_h v_h\} \cdot \llbracket v_h \rrbracket - \varepsilon \int_{\mathcal{F}_h^*} \frac{1}{\rho(x)} \{c^2 \nabla_h v_h\} \cdot \llbracket v_h \rrbracket \\ &\geq \frac{c^2}{\bar{\rho}} \|\nabla_h v_h\|_{0,\Omega}^2 + \frac{1}{\bar{\rho}} \|v_h\|_{0,\Omega}^2 + \mathbf{a}_{S,p} c^2 \|h_{\mathcal{F}}^{-1/2} \llbracket v_h \rrbracket\|_{0,\mathcal{F}_h^*}^2 + \frac{c^2(1-\varepsilon)}{\bar{\rho}} \int_{\mathcal{F}_h^*} \{ \nabla_h v_h \} \cdot \llbracket v_h \rrbracket \\ &\geq \frac{c^2}{\bar{\rho}} \|\nabla_h v_h\|_{0,\Omega}^2 + \frac{1}{\bar{\rho}} \|v_h\|_{0,\Omega}^2 + \mathbf{a}_{S,p} c^2 \|h_{\mathcal{F}}^{-1/2} \llbracket v_h \rrbracket\|_{0,\mathcal{F}_h^*}^2 \\ &\quad + \frac{c^2(1-\varepsilon)}{2\bar{\rho}} (-\|h_e^{1/2} \{ \nabla_h v_h \}\|_{0,\mathcal{F}_h^*}^2 - \|h_{\mathcal{F}}^{-1/2} \llbracket v_h \rrbracket\|_{0,\mathcal{F}_h^*}^2) \\ &\geq \underbrace{\min \left\{ \frac{1}{\bar{\rho}} \left(c^2 - C \left(\frac{1+\varepsilon}{2} \right) \right), \frac{1}{\bar{\rho}} \right\}}_{C_1} (\|\nabla_h v_h\|_{0,\Omega}^2 + \|v_h\|_{0,\Omega}^2) \\ &\quad + \underbrace{c^2 \left(\mathbf{a}_{S,p} - \left(\frac{1+\varepsilon}{2\bar{\rho}} \right) \right)}_{C_2} \|h_{\mathcal{F}}^{-1/2} \llbracket v_h \rrbracket\|_{0,\mathcal{F}_h^*}^2 \geq \alpha_p \|v_h\|_{DG}^2, \end{aligned}$$

where the constant C is the one provided by (3.1). Observe that, since $\nu > 0$, the ellipticity holds for $\nu > C(1+\varepsilon)/2$ and $\mathbf{a}_{S,p} > (1+\varepsilon)/2\bar{\rho}$, with $\varepsilon \in \{-1, 0, 1\}$. Hence, defining $\alpha_p := \min\{C_1, C_2\}$ and choosing \mathbf{a}_S such that $\mathbf{a}_{S,p} > \mathbf{a}_p^* := (1+\varepsilon)/2\bar{\rho}$ we conclude the proof. \square

Now, the discrete solution operator $T_h^{p,\varepsilon} : H^1(\Omega) \rightarrow \mathcal{V}_h^p$ is such that $T_h^{p,\varepsilon} f := \tilde{p}_h$ where \tilde{p}_h is the solution of the source problem $a_h(\tilde{p}_h, v_h) = b^p(f, v_h)$, for all $v_h \in \mathcal{V}_h^p$. In this formulation, $\varepsilon \in \{-1, 0, 1\}$ plays the same role as in the displacement formulation, providing symmetric or nonsymmetric DG methods.

Let us remark that, despite to the fact that the solution operator $T^{p,\varepsilon}$ is continuous and compact, the classic theory of [2] is not enough to our IPDG methods, since this theory requires that the numerical method must be conforming, implying that the noncompact theory of operators must be used for the pressure formulation. Then, properties P1 and P2 in this context reads as follows

- P1. $\|T^p - T_h^{p,\varepsilon}\|_{\mathcal{L}(\mathcal{V}_h^p, \mathcal{V}^p(h))} \rightarrow 0$ as $h \rightarrow 0$.
- P2. $\forall \tau \in \mathcal{V}_h^p$, there holds

$$\inf_{\tau \in \mathcal{V}_h^p} \|\tau - \tau_h\|_{\mathcal{V}^p(h)} \rightarrow 0 \quad \text{as } h \rightarrow 0.$$

The following convergence result holds for the continuous and discrete solution operators.

LEMMA 4.2. *For all $f \in \mathcal{V}^p$, the following estimate holds*

$$\|(T^p - T_h^{p,\varepsilon})f\|_{\mathcal{V}^p(h)} \lesssim h^s \|f\|_{0,\Omega},$$

with $s \in (1/2, 1]$ and the hidden constant is independent of h .

Proof. From the definition of the continuous and discrete solutions operators, we have $\widehat{p} := T^p f$ and $\widehat{p}_h := T_h^{p,\varepsilon} f$. Now, since \widehat{p}_h is the solution of the corresponding source problem, then $\|\widehat{p} - \widehat{p}_h\|_{\mathcal{V}^p(h)}$ is precisely the error of the DG method applied on the source problem. Then, the result follow with $s \in (1/2, 1]$. \square

If we consider discrete sources, we obtain the analogous of the previous lemma, in the sense that For all $f_h \in \mathcal{V}_h$, the following estimate holds

$$\|(T^p - T_h^{p,\varepsilon})f_h\|_{\mathcal{V}^p(h)} \lesssim h^s \|f_h\|_{\mathcal{V}^p(h)},$$

with $s \in (1/2, 1]$ and the hidden constant is independent of h . Now we are in position to establish P1.

LEMMA 4.3. *There following estimate holds*

$$\|T^p - T_h^{p,\varepsilon}\|_{\mathcal{L}(\mathcal{V}_h, \mathcal{V}^p(h))} \lesssim h^s,$$

where the hidden constant is independent of h .

Proof. Given $f_h \in \mathcal{V}_h^p$, we have

$$\|T - T_h^{p,\varepsilon}\|_{\mathcal{L}(\mathcal{V}_h^p, \mathcal{V}^p(h))} := \sup_{0 \neq f_h \in \mathcal{V}_h^p} \frac{\|(T^p - T_h^{p,\varepsilon})f_h\|_{\mathcal{V}^p(h)}}{\|f_h\|_{\mathcal{V}^p(h)}} \lesssim h^s.$$

This concludes the proof. \square

If $\mathcal{E}(\mathcal{V}^p)$ represents the invariant space for the eigenfunctions of the pressure formulation, such that if $p \in \mathcal{E}(\mathcal{V}^p)$ then $p \in H^{1+r}(\Omega)$ for $r > 0$ and $\mathcal{E}(\mathcal{V}_h^p)$ is its discrete counterpart, we are able to provide an error estimate for the eigenfunctions. To do this task, and taking into account that the pressure formulation is nothing else that the Laplacian operator, the arguments of [1] can be easily followed for our purposes.

LEMMA 4.4. *For h small enough it holds*

$$\widehat{\delta}_h(\mathcal{E}(\mathcal{V}^p), \mathcal{E}_h(\mathcal{V}_h^p)) \lesssim h^{\min\{r,k\}},$$

where the hidden constant is independent of h .

Finally we present error estimates for the eigenvalues for the symmetric and non-symmetric methods, where optimal and suboptimal order of convergence are attained, respectively.

THEOREM 4.5. *There exists a strictly positive constant h_0 such that, for $h < h_0$ there holds*

1. *If the symmetric IPDG method is considered ($\varepsilon = 1$), then there holds*

$$|\lambda - \lambda_h| \lesssim h^{2\min\{r,k\}},$$

2. *If any of the nonsymmetric IPDG methods are considered ($\varepsilon \in \{-1, 0\}$), then there holds*

$$|\lambda - \lambda_h| \lesssim h^{\min\{r,k\}},$$

where in each estimate the hidden constant is independent of h .

5. Numerical experiments. Now we report a series of numerical experiments in order to corroborate the robustness of the proposed method with $\varepsilon \in \{-1, 0, 1\}$. All the results have been obtained with a FEniCS script [16]. The computed order of convergence for the eigenvalues were obtained by means of a standard least square fitting. When no analytical solution is available, we compare the computed eigenvalues for each mesh with extrapolated values. Let us denote by N the refinement level of the mesh and λ the eigenvalues. For the experiments we consider three cases. In the first case, we study the influence of the stabilization parameter \mathbf{a} when the spectrum is computed, in order to observe the arising of spurious modes. This is an important analysis since, according to Lemma 3.3, the method is stable for a certain threshold of \mathbf{a} . Let us remark that this threshold changes when the configuration of the method changes, namely, physical constants, geometry of the domain, boundary conditions, etc. The second situation studies the convergence of the methods, where for $\varepsilon = 1$ the optimal order is expected, whereas for $\varepsilon \in \{-1, 0\}$ suboptimal order of convergence must be attained according to, for instance, [8, 20]. Finally, we consider domains with singularities and non-polygonal domains to observe the behavior of the method in these geometries.

Throughout this section, the stabilization parameter will be chosen proportional to the square of the polynomial degree k as $\mathbf{a}_S = \mathbf{a}k^2$, with $\mathbf{a} > 0$. We begin our report of numerical results considering first the discrete displacement formulation (3.2). Then, we will study the pure pressure numerical scheme (4.3).

From the results reported in [19, 20] for the elasticity and Stokes equations, respectively it follows that for $\mathbf{a} < 1$, the spurious eigenvalues appear more strongly compared with those computed when $\mathbf{a} > 1$. Therefore, considering that the coercivity constant depends on the density, in the spurious analysis experiments, we will present different combinations of stabilization parameters that depend on the lower and upper bounds of the density.

5.1. Test 1: Influence of the stabilization. In this experiment we test the effect of the stabilization parameter on each discontinuous scheme, namely SIP ($\varepsilon = 1$), IIP ($\varepsilon = 0$) and NIP ($\varepsilon = -1$). The importance of this study lies in determining which is the safest parameter to avoid pollution on the spectrum. To detect spurious modes, we compare eigenvalues and eigenfunctions.

The domain is the rectangle $\Omega := (0, a) \times (0, b)$. We choose $\rho_1(x, y) = \frac{1}{x^2 + y^2 + 1}$ and $\rho_2(x, y) = e^{xy+1}$, which correspond to density functions such that $|\rho_1(x, y)| \leq 1$ and $|\rho_2(x, y)| > 1$, respectively. For the experiment, we choose $a = 1$ and $b = 1.1$, whereas $c = 1$.

5.1.1. SIP method. In this test, we take $\varepsilon = 1$ in (3.3). The first goal is to study the influence of the stabilization parameter \mathbf{a}_S on the computation of the spectrum. More precisely, the intention is to analyze the appearance of spurious eigenvalues for certain values and localize a threshold in which the method is safe to compute the eigenvalues with physical meaning. In the forthcoming results, we report the computed eigenvalues fixing the refinement parameter N and taking different values of \mathbf{a} , and polynomial degrees. The numbers inside boxes represent spurious eigenvalues.

In Table 1 we note that spurious eigenvalues appear in the lowest order approximation for ρ_1 since $2(\bar{\rho} + \rho) < 4$, which is expected from the results in [20]. However, for ρ_2 we have a different scenario since $2(\bar{\rho} + \rho) \approx 21.7689$, but a spurious eigenvalue appears in the spectrum. Also, for this configuration of the problem, when the polynomial degree is increased, the appearance of spurious eigenvalues is less frequent. This

TABLE 1

Test 1. Computed eigenvalues $\lambda_{h,i}$ for polynomial degrees $k = 1, 2, 3$, mesh level $N = 8$ and different values of \mathbf{a} and $\rho(x)$, for the SIP method ($\varepsilon = 1$).

$k \backslash \mathbf{a}$	$\rho_1(x, y)$				$\rho_2(x, y)$			
	$2(\bar{\rho} + \underline{\rho})$	$4\bar{\rho}$	$4(\bar{\rho} + \underline{\rho})$	$8\bar{\rho}$	$2(\bar{\rho} + \underline{\rho})$	$4\bar{\rho}$	$4(\bar{\rho} + \underline{\rho})$	$8\bar{\rho}$
1	7.83005	7.85010	7.86139	7.87395	7.92006	7.93951	7.94676	7.95428
	9.58484	9.28119	9.64013	9.65956	10.29239	10.32611	10.33702	10.35267
	17.38317	10.02391	17.53053	17.60191	18.16105	18.28682	18.326917	18.36967
	26.83626	17.65229	32.78925	33.04550	32.91697	33.22771	33.41198	33.58185
	32.20629	32.68393	39.74527	40.03675	39.80118	40.23012	40.43040	40.62000
	39.05536	39.66805	42.43583	42.88156	41.68459	43.10124	43.38814	43.63388
	41.58004	42.41955	47.72058	48.27411	42.68574	48.74642	49.15382	49.52661
	46.71721	47.77799	72.84119	74.20859	48.66419	73.83369	74.61207	75.31965
	49.80943	72.54681	75.13436	76.53154	72.59414	75.71586	76.64642	77.55341
	70.17544	73.49931	84.38202	86.64709	74.59481	85.64420	87.01155	88.42254
2	7.83258	7.83261	7.83262	7.83263	7.91306	7.913092	7.913102	7.91312
	9.59294	9.59299	9.59300	9.59302	10.27004	10.27012	10.27016	10.27018
	17.42091	17.42146	17.42162	17.42179	18.16579	18.16631	18.16649	18.16666
	32.34693	32.34999	32.35098	32.35200	32.75789	32.76038	32.76132	32.76219
	39.15838	39.16262	39.16390	39.16518	39.60587	39.60917	39.61035	39.61145
	41.87547	41.88456	41.88704	41.88956	42.53659	42.54257	42.54459	42.54646
	47.03714	47.04933	47.05232	47.05533	47.98522	47.99580	47.99878	48.00148
	71.48122	71.53121	71.54302	71.55498	72.23229	72.26248	72.27162	72.28008
	73.16055	73.19808	73.20927	73.22068	73.57347	73.59884	73.60805	73.61669
	82.66712	82.75860	82.77748	82.79638	83.59049	83.65245	83.66898	83.68400
3	7.83253	7.83253	7.83253	7.83253	7.91295	7.91295	7.91295	7.91295
	9.59288	9.59288	9.59288	9.59288	10.26991	10.26991	10.26991	10.26992
	17.42060	17.42060	17.42060	17.42060	18.16508	18.16508	18.16508	18.16509
	32.34437	32.34437	32.34437	32.34438	32.75262	32.75263	32.75263	32.75264
	39.15584	39.15584	9.155855	39.15585	39.59998	39.59998	39.59998	39.59998
	41.87258	41.87260	41.87261	41.87262	42.52780	42.52781	42.52782	42.52784
	47.03552	47.03554	47.03555	47.03556	47.97646	47.97648	47.97649	47.97650
	71.47553	71.47572	71.47580	71.47587	72.19433	72.19446	72.19452	72.19457
	73.13334	73.13345	73.13350	73.13354	73.51695	73.51703	73.51707	73.51710
	82.66821	82.66852	82.66863	82.66875	83.53586	83.53609	83.53618	83.53628

fact allows us to infer that when the polynomial approximation increases, the spurious eigenvalues begin to vanish, at least when the lowest frequencies are considered.

From the above, one may be tempted to infer that the safe parameter for the SIP scheme is $\mathbf{a}\bar{\rho}$, for $\mathbf{a} \geq 4$. However, in Table 2 we observe an alternative spurious analysis, where we consider, in particular, stabilization parameters of the references [19, 20], together with a particular combination of the form $\mathbf{a}(\bar{\rho} + 1)$. Note the remarkable difference in the cleanliness of the spectrum between the schemes with ρ_1 and ρ_2 . In particular, the scheme with ρ_2 and $4(\bar{\rho} + 1)$, whose stabilized is larger compared to $4\bar{\rho}$, presented in the previous table, gives a spurious eigenvalue for $k = 1$. Moreover, we note that the safe parameters in the references are not sufficient if $|\rho(x, y)| > 1$. Therefore, we infer that the safe parameter choice for the SIP with variable density lies between the combinations $\mathbf{a}(\bar{\rho} + \underline{\rho})/2$ and $\mathbf{a}(\bar{\rho} + 1)$, for $\mathbf{a} \geq 8$, at least for the cases under study.

On the other hand, Tables 3–4 reveal that with the SIP method the optimal order of convergence is attained. More precisely, the order is exactly $\mathcal{O}(h^{2k})$. This order is obtained since the domain in which we state the problem is convex, leading to

TABLE 2

Test 1. Computed eigenvalues $\lambda_{h,i}$ for polynomial degrees $k = 1, 2, 3$, mesh level $N = 8$ and different values of \mathbf{a} and $\rho(x)$, for the SIP method ($\varepsilon = 1$).

$\begin{smallmatrix} \text{a} \\ \text{k} \end{smallmatrix}$	$\rho_1(x, y)$				$\rho_2(x, y)$			
	4	$4(\bar{\rho} + 1)$	8	$8(\bar{\rho} + 1)$	4	$4(\bar{\rho} + 1)$	8	$8(\bar{\rho} + 1)$
1	7.85010	7.87395	7.87395	7.88547	4.94719	7.94189	7.85203	7.95588
	9.28119	9.65956	9.65956	9.67768	7.73864	10.32434	10.15531	10.35597
	10.02391	17.60191	17.60191	17.66392	9.91112	18.29696	17.80452	18.37871
	17.65229	33.04550	33.04550	33.27389	15.58674	33.31167	29.18053	33.61829
	32.68393	40.03675	40.03675	40.29402	17.28392	40.31934	32.13420	40.66076
	39.66805	42.88156	42.88156	43.24050	27.92958	43.21682	37.94840	43.68507
	42.41955	48.27411	48.27411	48.73874	28.51991	48.86380	40.57725	49.60571
	47.77799	74.20859	74.20859	75.17274	33.30603	59.44931	44.65770	75.46235
	72.54681	76.53154	76.53154	77.73133	34.96146	74.52412	56.35742	77.74420
	73.49931	86.64709	86.64709	88.35366	36.65087	76.40702	65.81340	88.70701
2	7.83261	7.83263	7.83263	7.83264	7.91487	7.91309	7.91191	7.91312
	9.59299	9.59302	9.59302	9.59304	10.27009	10.27014	8.87486	10.27019
	17.42146	17.42179	17.42179	17.42194	18.15392	18.16639	10.26904	18.16669
	32.34999	32.35200	32.35200	32.35292	26.39878	32.76080	13.21076	32.76238
	39.16262	39.16518	39.16518	39.16633	32.75376	39.60970	17.28802	39.61168
	41.88456	41.88956	41.88956	41.89181	39.61667	42.54348	18.17024	42.54685
	47.04933	47.05533	47.05533	47.05800	42.52010	47.99715	32.75270	48.00205
	71.53121	71.55498	71.55498	71.56563	47.97542	72.26659	39.60443	72.28185
	73.19808	73.22068	73.22068	73.23088	53.28165	73.60296	42.53533	73.61851
	82.75860	82.79638	82.79638	82.81314	72.17575	83.65992	47.97276	83.68714
3	7.83253	7.83253	7.83253	7.83253	7.91295	7.91295	7.91295	7.91295
	9.59288	9.59288	9.59288	9.59288	10.26991	10.26991	10.26991	10.26991
	17.42060	17.42060	17.42060	17.42060	18.16508	18.16508	18.16508	18.16508
	32.34437	32.34438	32.34438	32.34438	31.51368	32.75263	32.75260	32.75263
	39.15584	39.15585	39.15585	39.15585	32.75255	39.59998	39.59995	39.59998
	41.87260	41.87262	41.87262	41.87263	39.59988	42.52782	42.52768	42.52783
	47.03554	47.03556	47.03556	47.03557	42.52740	47.97649	47.97635	47.97651
	71.47572	71.47587	71.47587	71.47594	47.97424	72.19448	72.19350	72.19458
	73.13345	73.13354	73.13354	73.13359	50.98591	73.51705	73.51650	73.51711
	82.66852	82.66875	82.66875	82.66885	72.19381	83.53613	83.53511	83.53630

sufficiently smooth eigenfunctions for our spectral problem.

5.1.2. NIP and IIP method. Now our aim is to study computationally the presence of spurious eigenvalues for the nonsymmetric methods, more precisely the NIP ($\varepsilon = -1$) and SIP ($\varepsilon = 0$). The combination of stabilization parameters are the same as those of SIP. In Table 5 we present the computed eigenvalues for different stabilizations and polynomial degrees when the NIP method is considered.

We observe that when the NIP method is performing the approximation of the spectrum with the selected stabilization parameters, there are no spurious eigenvalues arising for small values of \mathbf{a} . For ρ_1 , since $\bar{\rho} \geq 1$, we fall in the results presented in [20], whereas the scheme with density ρ_2 remains clean with $\bar{\rho} > 2$.

In contrast, we observe the results in Table 6, where a completely clean spectrum is observed for ρ_1 , while the spectrum with ρ_2 and $\mathbf{a} = 2, 4$, result in the computation of spurious eigenvalues. When we compare this behavior with the SIP method, we notice that the NIP method introduces more spurious modes compared with the SIP

TABLE 3

Test 1. Convergence analysis for $\mathbf{a} = 10(\bar{\rho} + 1)$, $\rho(x, y) = \frac{1}{x^2 + y^2 + 1}$, and $k = 1, 2, 3$ for the SIP method ($\varepsilon = 1$).

k	$N = 10$	$N = 20$	$N = 30$	$N = 40$	Order	λ_i
1	7.86806	7.84149	7.83652	7.83478	1.98	7.83248
	9.64947	9.60705	9.59919	9.59643	2.00	9.59290
	17.58538	17.46235	17.43923	17.43109	1.98	17.42052
	32.96979	32.50146	32.41428	32.38371	1.99	32.34399
2	7.83258	7.83253	7.83253	7.83253	3.99	7.83253
	9.59295	9.59289	9.59288	9.59288	3.99	9.59288
	17.42116	17.42063	17.42060	17.42060	3.98	17.42060
	32.34797	32.34457	32.34438	32.34435	3.97	32.34434
3	7.83253	7.83253	7.83253	7.83253	5.85	7.83253
	9.59288	9.59288	9.59288	9.59288	5.88	9.59288
	17.42060	17.42060	17.42060	17.42060	5.98	17.42060
	32.34435	32.34434	32.34434	32.34434	5.99	32.34434

TABLE 4

Test 1. Convergence analysis for $\mathbf{a} = 10(\bar{\rho} + 1)$, $\rho(x, y) = e^{xy+1}$, and $k = 1, 2, 3$ for the SIP method ($\varepsilon = 1$).

k	$N = 10$	$N = 20$	$N = 30$	$N = 40$	Order	λ_i
1	7.94234	7.92041	7.91628	7.91483	1.97	7.91291
	10.32857	10.28466	10.27648	10.27361	1.99	10.26989
	18.31292	18.20280	18.18194	18.17459	1.96	18.16476
	33.34798	32.90287	32.81956	32.79031	1.98	32.75189
2	7.91302	7.91296	7.912956	7.912956	3.99	7.91295
	10.27003	10.26992	10.26991	10.26991	3.99	10.26991
	18.16577	18.16512	18.16508	18.16508	3.98	18.16507
	32.75676	32.75285	32.75264	32.75260	3.97	32.75258
3	7.91295	7.91295	7.91295	7.91295	5.92	7.91295
	10.26991	10.26991	10.26991	10.26991	5.95	10.26991
	18.16508	18.16507	18.16507	18.16507	5.98	18.16507
	32.75260	32.75258	32.75258	32.75258	5.98	32.75258

method, for the same stabilization parameter. However, when the polynomial degree is increased, the NIP methods behaves better than the SIP method where for $\mathbf{a} \geq 4$

Let us remark that when the NIP method is considered, Table 6 shows that for $k = 1$ the number of spurious eigenvalues is clearly large compared for $k = 2$. Moreover, for $k = 3$ there is no visible spurious eigenvalues for any stabilization parameter. This has been also observed for $k = 4, 5, 6$. From these results, we infer that a safe parameter in which we can operate with the NIP method is for stabilizations such that $\mathbf{a} \geq 4$.

Now in Tables 7–8 we present convergence rates for the NIP method when different polynomial degrees are considered. From these tables, we observe that a suboptimal order of convergence is attained. More precisely, when k is odd, the order of convergence is $\mathcal{O}(h^k)$, whereas when k is even, the order of convergence is $\mathcal{O}(h^{k+1})$, which clearly is not optimal compared with the SIP method.

We remark that for the IIP method ($\varepsilon = 0$), the results related to the spurious analysis and order of convergence are similar to the NIP method. For the sake of brevity, we skip the results.

TABLE 5

Test 1. Computed eigenvalues $\lambda_{h,i}$ for polynomial degrees $k = 1, 2, 3$, mesh level $N = 8$ and different values of \mathbf{a} and $\rho(x)$, for the NIP ($\varepsilon = -1$) method.

$\begin{smallmatrix} \mathbf{a} \\ k \end{smallmatrix}$	$\rho_1(x, y)$				$\rho_2(x, y)$			
	$\bar{\rho} + \underline{\rho}$	$2\bar{\rho}$	$2(\bar{\rho} + \underline{\rho})$	$4\bar{\rho}$	$\bar{\rho} + \underline{\rho}$	$2\bar{\rho}$	$2(\bar{\rho} + \underline{\rho})$	$4\bar{\rho}$
1	7.74084	7.79239	7.81612	7.84287	7.89912	7.92612	7.93896	7.95100
	9.42728	9.50518	9.54304	9.58812	10.16304	10.22912	10.26408	10.30103
	16.84491	17.11841	17.24596	17.39284	17.90370	18.07698	18.16537	18.25622
	30.37398	31.33856	31.79499	32.32444	31.60803	32.30451	32.66855	33.05071
	36.67343	37.91183	38.46944	39.10970	38.24068	39.06090	39.49054	39.94433
	38.21148	39.99929	40.82734	41.74630	40.64388	41.81255	42.38055	42.94331
	43.61388	45.13923	45.90425	46.84143	45.58253	46.85679	47.56141	48.33365
	59.21923	65.54764	68.22675	70.98606	65.44416	69.58263	71.41674	73.13639
	63.44700	68.01181	70.23721	72.89916	67.67393	71.02756	72.85119	74.81097
	70.50419	75.99282	78.72432	82.06519	75.21822	79.64399	82.07951	84.72267
2	7.84646	7.84285	7.84091	7.83847	7.92746	7.92356	7.92134	7.91889
	9.61147	9.60681	9.60426	9.60101	10.29693	10.29000	10.28596	10.28140
	17.49628	17.47764	17.46744	17.45441	18.24717	18.22656	18.21449	18.20084
	32.64374	32.56841	32.52784	32.47677	33.02521	32.95571	32.91572	32.87114
	39.53666	39.44163	39.39020	39.32520	39.94652	39.85876	39.80801	39.75122
	42.36415	42.24515	42.18022	42.09761	42.95950	42.85318	42.79122	42.72144
	47.62310	47.48150	47.40405	47.30527	48.54451	48.40647	48.32566	48.23419
	72.84790	72.52868	72.35369	72.13023	73.37488	73.09611	72.93325	72.74945
	74.68225	74.30735	74.10584	73.85231	74.84721	74.52393	74.33815	74.13114
	84.65230	84.19038	83.93873	83.61867	85.32188	84.90646	84.66393	84.39006
3	7.83256	7.83255	7.83255	7.83254	7.91298	7.91297	7.91296	7.91296
	9.59293	9.59291	9.59291	9.59290	10.26997	10.26995	10.26994	10.26993
	17.42105	17.42093	17.42087	17.42079	18.16550	18.16538	18.16531	18.16524
	32.34726	32.34647	32.34607	32.34556	32.75509	32.75440	32.75402	32.75360
	39.15956	39.15856	39.15803	39.15738	39.60313	39.60225	39.60176	39.60122
	41.87933	41.87756	41.87662	41.87545	42.53310	42.53165	42.53083	42.52994
	47.04380	47.04165	47.04051	47.03908	47.98422	47.98215	47.98097	47.97967
	71.50754	71.49928	71.49490	71.48939	72.21964	72.21292	72.20910	72.20487
	73.16741	73.15827	73.15349	73.14759	73.54462	73.53705	73.53280	73.52813
	82.72109	82.70733	82.70006	82.69098	83.58124	83.56921	83.56237	83.55478

5.2. Test 2. A 2D reactor. This experiment aims to show the performance of the scheme when there is a non-polygonal domain and the density $\rho(x)$ is non constant. This implies that a priori we have zones within the domain where the fluid density is higher or lower. The considered domain is given by $\Omega := \tilde{\Omega} \setminus \bigcup_{i=1}^4 \Omega_i$, where

$$\tilde{\Omega} := \{(x, y) \in \mathbb{R}^2 : x^2 + y^2 \leq 1\},$$

$$\Omega_i := \left\{ (x, y) \in \mathbb{R}^2 : \left(x + \frac{1}{3}a\right)^2 + \left(y + \frac{1}{3}b\right)^2 < \frac{1}{8} \right\},$$

with $a = (-1)^i$ and $b = (-1)^{\frac{i(i-1)}{2}+1}$, for $i = 1, 2, 3, 4$. This domain resembles a cross-section of a reactor. The domain is meshed such that $h \approx 1/2^N$, with $N = 3, 4, 5, 6$. For a clean spectrum, we choose the stabilization parameter $\mathbf{a} = 20$. It notes that the expected order of convergence of the eigenvalues is $\mathcal{O}(h^2)$. This is due to the variational crime that is committed when a curved domain is approximated by polygons. This fact has been also observed in [20].

In Figure 1 we report the experimental convergence obtained by least squares fitting, solving the problem using the SIP and NIP scheme. Here, `dof` denotes the

TABLE 6

Test 1. Computed eigenvalues $\lambda_{h,i}$ for polynomial degrees $k = 1, 2, 3$, mesh level $N = 8$ and different values of α and $\rho(x)$, for the NIP ($\varepsilon = -1$) method.

k \ a	$\rho_1(x, y)$				$\rho_2(x, y)$			
	2	$2(\bar{\rho} + 1)$	4	$4(\bar{\rho} + 1)$	2	$2(\bar{\rho} + 1)$	4	$4(\bar{\rho} + 1)$
1	7.79239	7.84287	7.84287	7.86916	7.50961	7.93180	7.751918	7.95346
	9.50518	9.58812	9.58812	9.63647	9.41399	10.24419	9.85755	10.30940
	17.11841	17.3928	17.3928	17.54436	15.58637	18.11537	17.02452	18.27644
	31.33856	32.32444	32.32444	32.87046	20.20981	32.46180	28.30139	33.13710
	37.91183	39.10970	39.10970	39.77174	22.88114	39.24633	33.68424	40.04751
	39.99929	41.74630	41.74630	42.63479	24.96308	42.06174	34.82433	43.06573
	45.13923	46.84143	46.84143	47.87919	26.94440	47.15775	38.22918	48.51337
	65.54764	70.98606	70.98606	73.47962	28.69336	70.40197	40.38647	73.50271
	68.01180	72.89916	72.89916	75.69995	29.71622	71.80870	45.80849	75.25708
	75.99282	82.06519	82.06519	85.68356	30.54102	80.68556	52.33948	85.33071
2	7.84285	7.83847	7.83847	7.83579	7.11555	7.92261	7.94064	7.94064
	9.60680	9.60101	9.60101	9.59739	7.93392	10.28829	10.31911	10.28033
	17.47764	17.45441	17.45441	17.43976	10.27103	18.22145	18.31268	18.19761
	32.56841	32.47677	32.47677	32.42035	18.17500	32.93874	33.25550	32.86073
	39.44163	39.32520	39.32520	39.25305	32.71864	39.83724	40.23387	39.73792
	42.24515	42.09761	42.09761	42.00507	39.60958	42.82695	43.30082	42.70503
	47.48150	47.30527	47.30527	47.19430	42.28333	48.37230	48.98499	48.21260
	72.52868	72.13023	72.13023	71.87892	47.90767	73.02722	74.26323	72.70616
	74.30735	73.85231	73.85231	73.57203	50.66857	74.44508	75.92709	74.08280
	84.19038	83.61866	83.61866	83.26009	71.03522	84.80387	86.65687	84.32550
3	7.83255	7.83254	7.83254	7.83253	7.91308	7.91297	7.91302	7.91296
	9.59291	9.59290	9.59290	9.59289	10.27009	10.26995	10.27003	10.26993
	17.42093	17.42079	17.42079	17.42070	18.16644	18.16535	18.16597	18.16523
	32.34647	32.34556	32.34556	32.34501	32.76030	32.75424	32.75768	32.75350
	39.15855	39.15738	39.15738	39.15668	39.60958	39.60204	39.60637	39.60110
	41.87755	41.87545	41.87545	41.87417	42.54384	42.53130	42.53849	42.52973
	47.04165	47.03908	47.03908	47.03749	47.99840	47.98165	47.99156	47.97936
	71.49928	71.48939	71.48939	71.48330	72.26535	72.21129	72.24347	72.20388
	73.15827	73.14759	73.14759	73.14115	73.59971	73.53524	73.57238	73.52705
	82.70733	82.69098	82.69098	82.68094	83.66459	83.56630	83.62420	83.55301

number of degrees of freedom, whereas the error on the i -th eigenvalue is denoted by $\text{err}(\lambda_i)$, with

$$\text{err}(\lambda_i) := |\lambda_{h_i} - \lambda_i|.$$

For the IIP method, the values obtained were similar to those obtained with NIP. Note that in all cases, the order of convergence remains as predicted theoretically, for all selected fluid densities. This is followed by Figure 2, where we show the eigenfunctions associated to the first eigenvalue for each density function. Note that the fluid particles tend to move faster in the lower density zones, as expected. It is worth noting that, when using the NIP method, the spectrum may contain complex values, so we have only reported the real part of the spectrum. These complex contributions can appear at any place and any refinement. For example, for $\rho(x, y) = 1/[\cos(\pi x) \cos(\pi y) + 2]$ and $N = 3$, the first two computed eigenvalues are of the form $\lambda_h = 3.47649 \pm 0.00009i$.

TABLE 7

Test 1. Convergence analysis for $\mathbf{a} = 10(\bar{\rho} + 1)$, $\rho(x, y) = \frac{1}{x^2 + y^2 + 1}$, and $k = 1, 2, 3$ for the NIP method ($\varepsilon = -1$).

k	$N = 10$	$N = 20$	$N = 30$	$N = 40$	Order	λ_i
1	7.86660	7.84112	7.83636	7.83468	1.99	7.83253
	9.64235	9.60531	9.59842	9.59600	1.99	9.59286
	17.56622	17.45746	17.43704	17.42986	1.98	17.42050
	32.91484	32.48800	32.40836	32.38040	1.99	32.34428
2	7.83341	7.83273	7.83262	7.83258	2.16	7.83253
	9.59410	9.59316	9.59300	9.59295	2.16	9.59289
	17.42594	17.42177	17.42110	17.42087	2.23	17.42064
	32.36612	32.34895	32.34630	32.34542	2.29	32.34454
3	7.83253	7.83253	7.83253	7.83253	4.10	7.83253
	9.59288	9.59288	9.59288	9.59288	4.08	9.59288
	17.42061	17.42060	17.42060	17.42060	4.14	17.42060
	32.34446	32.34434	32.34434	32.34434	4.15	32.34434

TABLE 8

Test 1. Convergence analysis for $\mathbf{a} = 10(\bar{\rho} + 1)$, $\rho(x, y) = e^{xy+1}$, and $k = 1, 2, 3$ for the NIP method ($\varepsilon = -1$).

k	$N = 10$	$N = 20$	$N = 30$	$N = 40$	Order	λ_i
1	7.94590	7.92131	7.91668	7.91505	1.98	7.91294
	10.32299	10.28334	10.27591	10.27329	1.98	10.26988
	18.30356	18.20050	18.18092	18.17402	1.96	18.16484
	33.28860	32.88857	32.81330	32.78681	1.97	32.75168
2	7.91440	7.91328	7.91309	7.91303	2.16	7.91296
	10.27278	10.27057	10.27020	10.27007	2.14	10.26993
	18.17420	18.16711	18.16595	18.16556	2.19	18.16513
	32.78360	32.75927	32.75544	32.75417	2.25	32.75282
3	7.91295	7.91295	7.91295	7.91295	4.25	7.91295
	10.26992	10.26991	10.26991	10.26991	4.20	10.26991
	18.16510	18.16508	18.16507	18.16507	4.22	18.16507
	32.75274	32.75259	32.75258	32.75258	4.17	32.75258

5.3. Test 3: A 3D torus. This test aims to assess the DG method on a three dimensional non-polygonal domain. We consider a torus azimuthally symmetric about the z -axis, whose domain is characterized by

$$\Omega := \left\{ (x, y, z) \in \mathbb{R}^3 : \left(\sqrt{x^2 + y^2} - R \right)^2 + z^2 = r^2 \right\},$$

where $R = 1/2$ and $r = 1/4$. For simplicity, the physical parameters are taken equal to 1. In Table 9 we observe that for the lowest order, the variants of our discontinuous scheme converge with quadratic order, as the theory predicts. This is due to the fact that the eigenfunctions in this domain are regular. However, a variational crime is also being committed when approximating this domain with polyhedrons, so this order will not to improve for $k > 1$. Finally, in Figures 3 and 4 we depict the velocity field along with the post-processed pressure for the third and fifth eigenmodes.

6. Test 4. The pressure formulation. Since $\varepsilon \in \{-1, 0, 1\}$ as in the displacement formulation, for the pressure formulation we analyze the spurious behavior when the DG method is considered. The domain, physical parameters and eigenvalues are

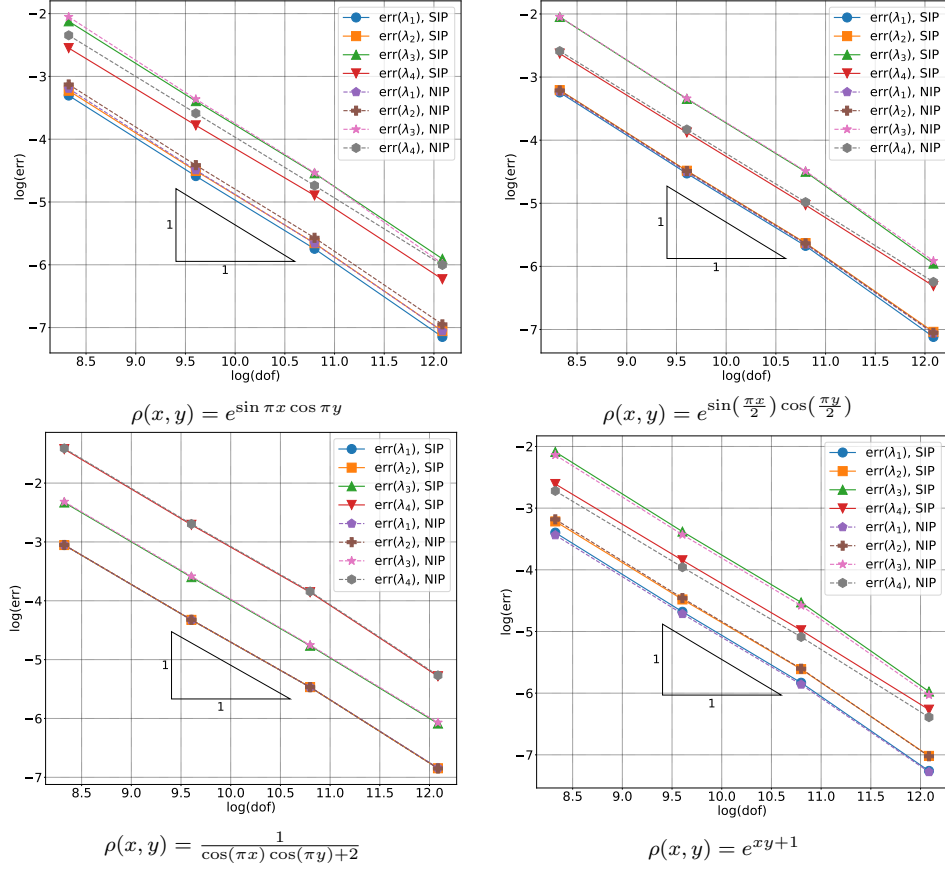


FIG. 1. Test 2. Error curves for the first four lowest computed eigenvalues when using different density functions.

TABLE 9
Test 3. Lowest computed eigenvalues for $k=1$, and $a=10$ for the SIP, NIP and IIP method.

method	$N=15$	$N=20$	$N=25$	$N=30$	Order	λ_{extr}
SIP	4.20546	4.20096	4.19911	4.19778	1.97	4.19504
	4.20588	4.20127	4.19923	4.19794	1.94	4.19497
	15.90982	15.87822	15.86392	15.85563	2.00	15.83625
	15.91094	15.87873	15.86493	15.85597	2.00	15.83658
	33.31118	33.20592	33.15811	33.12984	1.96	33.06265
NIP	4.20528	4.20086	4.19904	4.19774	1.98	4.19506
	4.20571	4.20117	4.19917	4.19789	1.94	4.19497
	15.90732	15.87681	15.86295	15.85497	1.99	15.83604
	15.90853	15.87728	15.86398	15.85527	2.01	15.83669
	33.30065	33.19987	33.15391	33.12693	1.96	33.06252
IIP	4.20535	4.20090	4.19907	4.19775	1.97	4.19503
	4.20577	4.20121	4.19920	4.19791	1.94	4.19497
	15.90892	15.87736	15.86333	15.85523	2.00	15.83624
	15.90946	15.87784	15.86435	15.85554	2.00	15.83653
	33.30471	33.20221	33.15554	33.12806	1.96	33.06259

the same as those of Test 1. In Tables 10–11 we report the computed eigenvalues

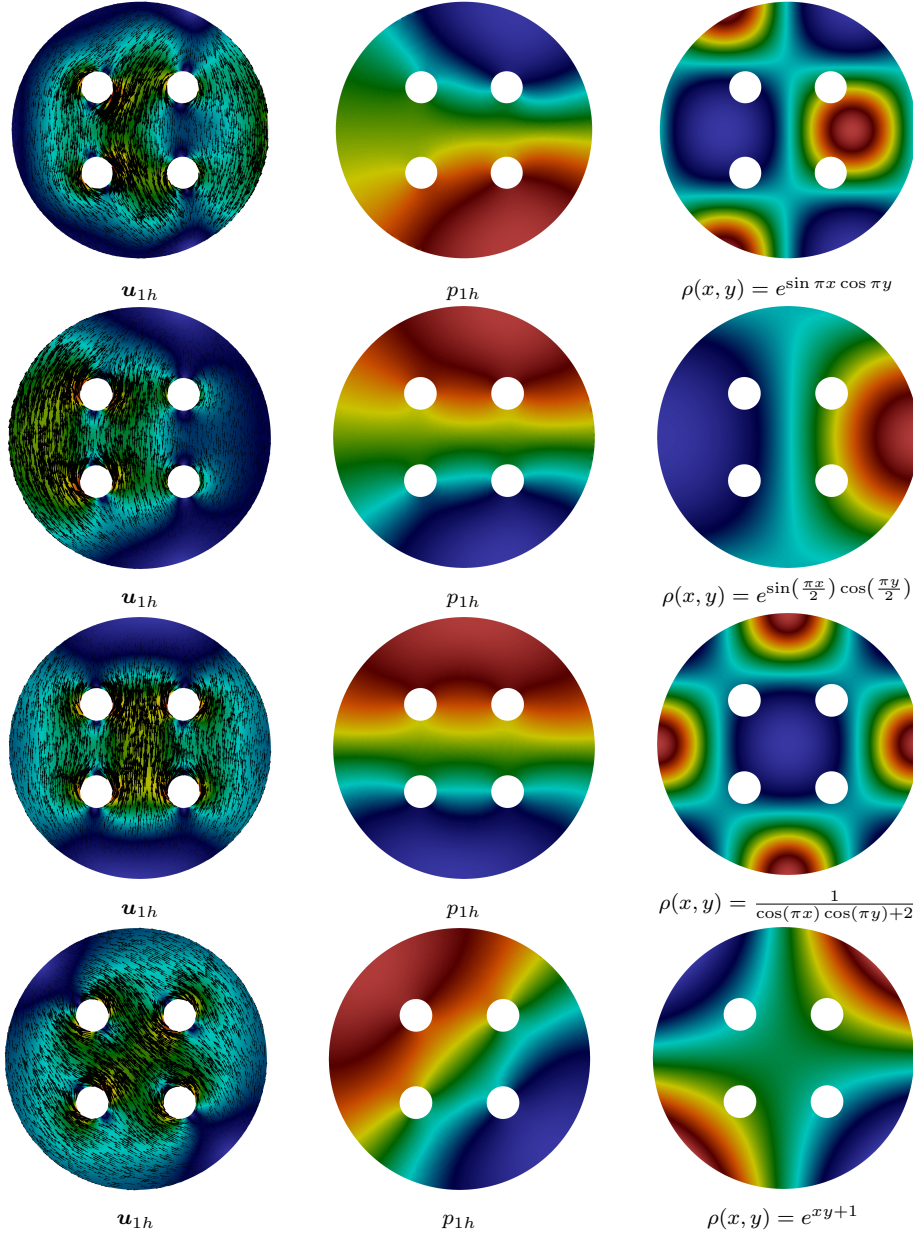


FIG. 2. *Test 2. Lowest computed eigenmodes and postprocessed pressure using different density functions.*

obtained with the SIP method, fixing the mesh refinement in $N = 8$ and considering different polynomial degrees and values of \mathbf{a} . We observe that the results are similar compared with those on Tables 1–2. However, for the smallest stabilization parameters, the pressure formulation gives more spurious eigenvalues when the polynomial degree is $k = 1$.

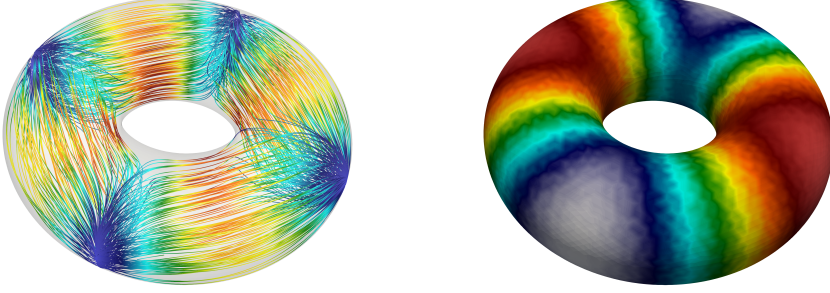


FIG. 3. *Test 3. Third lowest computed eigenmode \mathbf{u}_h streamlines (left) and postprocessed pressure (right).*

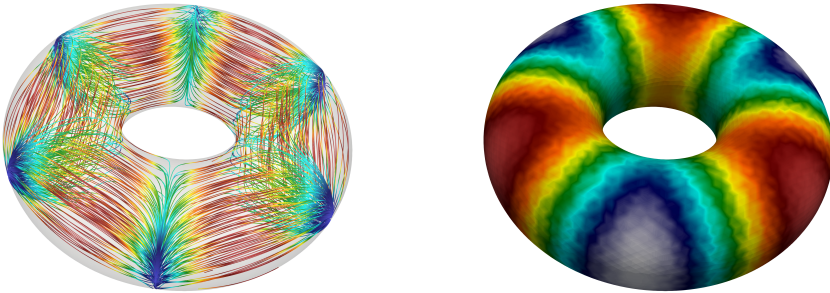


FIG. 4. *Test 3. Fifth lowest computed eigenmode \mathbf{u}_h streamlines (left) and postprocessed pressure (right).*

7. Test 5. A 3D benchmark. In order to obtain more information of the discrete formulations (3.2) and (4.3), now we compare some aspects of the computational cost of these schemes. To achieve this goal, we resort to the debug report delivered by FENICS through the command `set_log_level(LogLevel.DEBUG)`, where we can recover several debug information, among them, the assembly time, the non-zero entries of the assembled matrices and the sparsity percentage. We solve the eigenproblems in the unit cube $\Omega := (0, 1)^2$ using uniform refinements, where the number of cells scales as $6(N + 1)^3$. It is clear that for the cases studied, the generalized eigenvalue system is of the form $\mathbf{K}_u \mathbf{u} = \lambda \mathbf{M}_u \mathbf{u}$ for (3.2) and $\mathbf{K}_p p = \lambda \mathbf{M}_p p$ for (4.3). In this experiment, we denote by $K_{0,u}$ and $M_{0,u}$ the number of non-zero entries of \mathbf{K}_u and \mathbf{M}_u in each refinement. Similarly, we denote by $K_{0,p}$ and $M_{0,p}$ the number of non-zero entries of \mathbf{K}_p and \mathbf{M}_p . In Figure 5 can observe the behavior of the assembly and solution times, in seconds, of the eigenvalue system in both cases, taken as the average of 5 continuous runs. It is clear that solving (4.3) is considerably cheaper, mainly because of the number of degrees of freedom (dof) in the problem. This is followed by the results depicted in Figure 6, where we observe the number of non-zero inputs with respect to the number of degrees of freedom, and also the ratio between the non-zero inputs and dof^2 . The y -axis scale is measured with the logarithm of the computed values. Note that the ratio between non-zero entries and dof^2 of the matrices associated with (4.3) are lower than those of (3.2), which is expected since (4.3) is associated with fewer degrees of freedoms.

8. Conclusions. We have presented DG methods to approximate the eigenvalues and eigenfunctions of the acoustic eigenvalue problem. The proposed symmetric

TABLE 10

Test 4. Computed eigenvalues $\lambda_{h,i}$ for polynomial degrees $k = 1, 2, 3$, mesh level $N = 8$ and different values of \mathbf{a} and $\rho(x)$, for the SIP method ($\varepsilon = 1$).

$\begin{smallmatrix} \text{a} \\ k \end{smallmatrix}$	$\rho_1(x, y)$				$\rho_2(x, y)$			
	$2(\bar{\rho} + \underline{\rho})$	$4\bar{\rho}$	$4(\bar{\rho} + \underline{\rho})$	$8\bar{\rho}$	$2(\bar{\rho} + \underline{\rho})$	$4\bar{\rho}$	$4(\bar{\rho} + \underline{\rho})$	$8\bar{\rho}$
1	7.85831	7.87585	6.28236	7.89707	8.00791	8.00878	8.00921	8.00965
	9.61673	9.64631	7.99171	9.66568	10.39198	10.39333	10.39401	10.39470
	11.12628	14.56096	9.65834	17.78279	18.81280	18.82297	18.82815	18.83341
	17.58573	17.70166	17.72448	33.38125	34.38199	34.39806	34.40617	34.41436
	32.74643	33.05492	33.12913	40.25775	41.54168	41.56437	41.57583	41.58741
	35.66546	37.81773	40.04185	43.71383	45.60117	45.64630	45.66926	45.69258
	39.50152	40.23103	42.42326	49.10155	52.15709	52.22394	52.25799	52.29260
	42.56402	43.36561	46.34274	76.38572	81.30052	81.44241	81.51355	81.58492
	47.59880	48.28572	51.09714	78.06806	81.90845	82.01209	82.06557	82.12053
	57.83388	56.48285	72.73759	89.46875	96.68894	96.89340	96.99754	97.10336
2	7.83258	7.83261	7.83264	7.83269	7.91319	7.91319	7.91320	7.91320
	9.59304	9.59295	9.59300	9.59306	10.27022	10.27022	10.27023	10.27023
	17.42250	17.42202	17.42253	17.42303	18.16847	18.16851	18.16853	18.16854
	32.34518	32.34930	32.35180	32.35447	32.76848	32.76863	32.76870	32.76877
	39.14741	39.15855	39.16265	39.16658	39.61886	39.61907	39.61917	39.61928
	41.88102	41.89014	41.89664	41.90275	42.56796	42.56834	42.56853	42.56872
	47.02938	47.05119	47.06061	47.06864	48.03134	48.03189	48.03216	48.03244
	65.11345	71.55640	71.59582	71.62566	72.39744	72.39937	72.40035	72.40134
	71.73920	73.19101	73.21856	73.24738	73.69022	73.69170	73.69245	73.69320
	73.17229	82.78775	82.83178	82.87428	83.84312	83.84562	83.84688	83.84816
3	7.83253	7.83253	7.83253	7.83253	7.91295	7.91295	7.91295	7.91295
	9.59288	9.59288	9.59288	9.59288	10.26991	10.26991	10.26991	10.26991
	17.42060	17.42060	17.42060	17.42060	18.16508	18.16508	18.16508	18.16508
	32.34439	32.34439	32.34440	32.34440	32.75265	32.75265	32.75265	32.75265
	39.15585	39.15586	39.15587	39.15587	39.60000	39.60000	39.60000	39.60000
	41.87267	41.87270	41.87272	41.87274	42.52793	42.52793	42.52793	42.52793
	47.03560	47.03564	47.03566	47.03568	47.97662	47.97662	47.97662	47.97662
	71.47621	71.47651	71.47664	71.47679	72.19550	72.19551	72.19551	72.19551
	73.13362	73.13384	73.13394	73.13406	73.51765	73.51766	73.51766	73.51766
	82.66900	82.66951	82.66975	82.67002	83.53781	83.53783	83.53784	83.53784

and nonsymmetric methods lead to an accurate computation and approximation of the corresponding eigenfunctions. The acoustic problem has as unknowns the displacement and pressure of the fluid. These DG methods were considered for two formulations: a formulation where the displacement is the only unknown and other where the pressure is the unknown. For both approaches, the remaining unknown is always recovered with a postprocess of the solution operator under study. A spurious analysis is presented in two dimensions, where we compare the effects of the stabilization parameter in the symmetric and nonsymmetric methods when the spectrum is computed, performing both the displacement and pressure formulations. The numerical tests also reveal that, for a correct choice of the aforementioned stabilization, the convergence order is the expected in two and three dimensions. On the other hand, a benchmark test shows that the pressure formulation is less expensive in terms of computational costs compared with the displacement formulation. This conclusion is expectable since the pure pressure problem is only scalar. However, in both formulations, the eigenvalues are exactly the same, together with the computed convergence orders for both, the symmetric or nonsymmetric approaches.

TABLE 11

Test 4. Computed eigenvalues $\lambda_{h,i}$ for polynomial degrees $k = 1, 2, 3$, mesh level $N = 8$ and different values of \mathbf{a} and $\rho(x)$, for the SIP method ($\varepsilon = 1$).

k \ a	$\rho_1(x, y)$				$\rho_2(x, y)$			
	4	$4(\bar{\rho} + 1)$	8	$8(\bar{\rho} + 1)$	4	$4(\bar{\rho} + 1)$	8	$8(\bar{\rho} + 1)$
1	7.87585	7.89707	7.89707	7.91503	7.99747	8.00897	8.00365	8.00975
	9.64631	9.66568	9.66568	9.68920	10.37575	10.39362	10.38534	10.39485
	14.56096	17.78279	17.78279	17.89578	18.69974	18.82522	18.76446	18.83457
	17.70166	33.38125	33.38125	33.66847	34.18685	34.40160	34.30248	34.41615
	33.05492	40.25775	40.25775	40.66849	41.26919	41.56936	41.43004	41.58995
	37.81773	43.71383	43.71383	44.32293	45.09283	45.65629	45.38552	45.69770
	40.23103	49.10155	49.10155	49.89565	51.41133	52.23875	51.83909	52.30021
	43.36561	76.38572	76.38572	78.37028	79.63021	81.47347	80.59982	81.60048
	48.28572	78.06806	78.06806	79.75233	80.75383	82.03530	81.42428	82.13270
2	56.48285	89.46875	89.46875	92.09170	94.40090	96.93872	95.71525	97.12663
	7.83261	7.83269	7.83269	7.83273	7.91316	7.91320	7.91318	7.91320
	9.59295	9.59306	9.59306	9.59312	10.27018	10.27022	10.27020	10.27023
	17.42202	17.42303	17.42303	17.42357	18.16806	18.16852	18.16830	18.16855
	32.34930	32.35447	32.35447	32.35720	32.76667	32.76866	32.76775	32.76879
	39.15855	39.16658	39.16658	39.17049	39.61629	39.61911	39.61782	39.61930
	41.89014	41.90275	41.90275	41.90920	42.56350	42.56842	42.56612	42.56876
	47.05119	47.06864	47.06864	47.07696	48.02489	48.03201	48.02868	48.03250
	71.55640	71.62566	71.62566	71.65676	72.37484	72.39979	72.38805	72.40155
3	73.19101	73.24738	73.24738	73.27627	73.67168	73.69203	73.68279	73.69336
	82.78775	82.87428	82.87428	82.91733	83.81269	83.84617	83.83073	83.84844
	7.83253	7.83253	7.83253	7.83253	7.91295	7.91295	7.91295	7.91295
	9.59288	9.59288	9.59288	9.59288	10.26991	10.26991	10.26991	10.26991
	17.42060	17.42060	17.42060	17.42060	18.16508	18.16508	18.16508	18.16508
	32.34439	32.34440	32.34440	32.34441	32.75264	32.75265	32.75264	32.75265
	39.15586	39.15587	39.15587	39.15588	39.60000	39.60000	39.60000	39.60000
	41.87270	41.87274	41.87274	41.87275	42.52792	42.52793	42.52793	42.52793
	47.03564	47.03568	47.03568	47.03570	47.97660	47.97662	47.97661	47.97662
	71.47651	71.47679	71.47679	71.47695	72.19541	72.19551	72.19546	72.19551
	73.13384	73.13406	73.13406	73.13419	73.51757	73.51766	73.51762	73.51766
	82.66951	82.67002	82.67002	82.67031	83.53763	83.53783	83.53774	83.53784

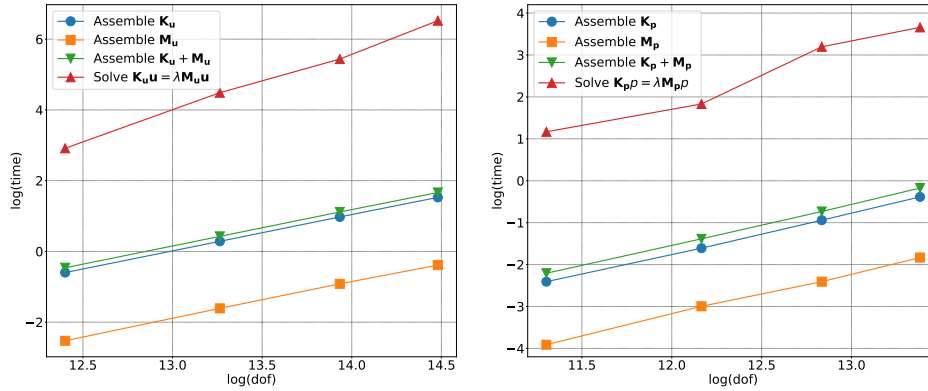


FIG. 5. Test 5. Comparison of time employed by the velocity and pressure schemes when assembling and solving the eigenproblems in a 3D unit cube with uniform refinements. Left: velocity formulation. Right: pure pressure formulation.

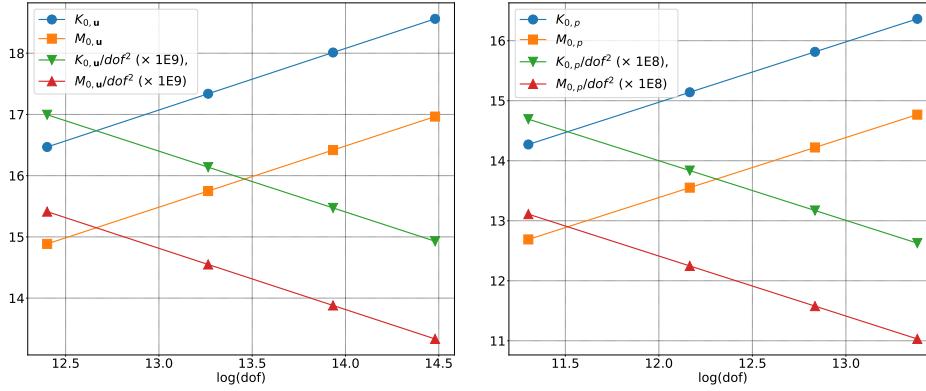


FIG. 6. Test 5. Comparison of the sparsity in the the velocity and pressure schemes on each mesh level for the 3D unit cube with uniform refinements. Left: velocity formulation. Right: pure pressure formulation.

REFERENCES

- [1] P. F. ANTONIETTI, A. BUFFA, AND I. PERUGIA, *Discontinuous Galerkin approximation of the Laplace eigenproblem*, Comput. Methods Appl. Mech. Engrg., 195 (2006), pp. 3483–3503, <https://doi.org/10.1016/j.cma.2005.06.023>.
- [2] I. BABUŠKA AND J. OSBORN, *Eigenvalue problems*, in Handbook of numerical analysis, Vol. II, Handb. Numer. Anal., II, North-Holland, Amsterdam, 1991, pp. 641–787.
- [3] Y. BAI AND Q. BAI, *Subsea pipeline integrity and risk management*, Gulf Professional Publishing, 2014.
- [4] L. BEIRÃO DA VEIGA, D. MORA, G. RIVERA, AND R. RODRÍGUEZ, *A virtual element method for the acoustic vibration problem*, Numer. Math., 136 (2017), pp. 725–763, <https://doi.org/10.1007/s00211-016-0855-5>.
- [5] A. BERMÚDEZ, R. DURÁN, M. A. MUSCHIETTI, R. RODRÍGUEZ, AND J. SOLOMIN, *Finite element vibration analysis of fluid-solid systems without spurious modes*, SIAM J. Numer. Anal., 32 (1995), pp. 1280–1295, <https://doi.org/10.1137/0732059>.
- [6] A. BERMÚDEZ, P. GAMALLO, AND R. RODRÍGUEZ, *Finite element methods in local active control of sound*, SIAM J. Control Optim., 43 (2004), pp. 437–465, <https://doi.org/10.1137/S0363012903431785>.
- [7] A. BERMÚDEZ, R. RODRÍGUEZ, AND D. SANTAMARINA, *Two discretization schemes for a time-domain dissipative acoustics problem*, Math. Models Methods Appl. Sci., 16 (2006), pp. 1559–1598, <https://doi.org/10.1142/S0218202506001637>.
- [8] A. BUFFA, P. HOUSTON, AND I. PERUGIA, *Discontinuous Galerkin computation of the Maxwell eigenvalues on simplicial meshes*, J. Comput. Appl. Math., 204 (2007), pp. 317–333, <https://doi.org/10.1016/j.cam.2006.01.042>.
- [9] A. BUFFA AND I. PERUGIA, *Discontinuous Galerkin approximation of the Maxwell eigenproblem*, SIAM J. Numer. Anal., 44 (2006), pp. 2198–2226, <https://doi.org/10.1137/050636887>.
- [10] A. BUFFA, I. PERUGIA, AND T. WARBURTON, *The mortar-discontinuous Galerkin method for the 2D Maxwell eigenproblem*, J. Sci. Comput., 40 (2009), pp. 86–114, <https://doi.org/10.1007/s10915-008-9238-0>.
- [11] J. DESCLOUX, N. NASSIF, AND J. RAPPAPAZ, *On spectral approximation. I. The problem of convergence*, RAIRO Anal. Numér., 12 (1978), pp. 97–112, iii, <https://doi.org/10.1051/m2an/1978120200971>.
- [12] J. DESCLOUX, N. NASSIF, AND J. RAPPAPAZ, *On spectral approximation. II. Error estimates for the Galerkin method*, RAIRO Anal. Numér., 12 (1978), pp. 113–119, iii, <https://doi.org/10.1051/m2an/1978120201131>.
- [13] D. A. DI PIETRO AND A. ERN, *Mathematical aspects of discontinuous Galerkin methods*, vol. 69 of Mathématiques & Applications (Berlin) [Mathematics & Applications], Springer, Heidelberg, 2012, <https://doi.org/10.1007/978-3-642-22980-0>.
- [14] E. HERNÁNDEZ AND R. RODRÍGUEZ, *Finite element approximation of spectral acoustic problems on curved domains*, Numer. Math., 97 (2004), pp. 131–158, <https://doi.org/10.1007/s00211-003-0501-x>.

- [15] T. KIRSTEIN, *Multidisciplinary know-how for smart-textiles developers*, Elsevier, 2013.
- [16] H. P. LANGTANGEN AND A. LOGG, *Solving PDEs in Python*, vol. 3 of Simula SpringerBriefs on Computing, Springer, Cham, 2016, <https://doi.org/10.1007/978-3-319-52462-7>. The FEniCS tutorial I.
- [17] W. LARBI, J.-F. DEÛ, AND R. OHAYON, *A new finite element formulation for internal acoustic problems with dissipative walls*, Internat. J. Numer. Methods Engrg., 68 (2006), pp. 381–399, <https://doi.org/10.1002/nme.1727>.
- [18] F. LEPE, S. MEDDAHI, D. MORA, AND R. RODRÍGUEZ, *Acoustic vibration problem for dissipative fluids*, Math. Comp., 88 (2019), pp. 45–71, <https://doi.org/10.1090/mcom/3336>.
- [19] F. LEPE, S. MEDDAHI, D. MORA, AND R. RODRÍGUEZ, *Mixed discontinuous Galerkin approximation of the elasticity eigenproblem*, Numer. Math., 142 (2019), pp. 749–786, <https://doi.org/10.1007/s00211-019-01035-9>.
- [20] F. LEPE AND D. MORA, *Symmetric and nonsymmetric discontinuous Galerkin methods for a pseudostress formulation of the Stokes spectral problem*, SIAM J. Sci. Comput., 42 (2020), pp. A698–A722, <https://doi.org/10.1137/19M1259535>.
- [21] F. LEPE AND G. RIVERA, *A virtual element approximation for the pseudostress formulation of the Stokes eigenvalue problem*, Comput. Methods Appl. Mech. Engrg., 379 (2021), pp. Paper No. 113753, 21, <https://doi.org/10.1016/j.cma.2021.113753>.
- [22] A. MÁRQUEZ, S. MEDDAHI, AND T. TRAN, *Analyses of mixed continuous and discontinuous Galerkin methods for the time harmonic elasticity problem with reduced symmetry*, SIAM J. Sci. Comput., 37 (2015), pp. A1909–A1933, <https://doi.org/10.1137/14099022X>.
- [23] D. MORA, G. RIVERA, AND R. RODRÍGUEZ, *A virtual element method for the Steklov eigenvalue problem*, Math. Models Methods Appl. Sci., 25 (2015), pp. 1421–1445, <https://doi.org/10.1142/S0218202515500372>.
- [24] R. OSIANDER AND A. DARRIN, *Wireless mems for space applications*, in Wireless MEMS Networks and Applications, Elsevier, 2017, pp. 197–214.
- [25] J. QUERALES, R. RODRÍGUEZ, AND P. VENEGAS, *Numerical approximation of the displacement formulation of the axisymmetric acoustic vibration problem*, SIAM J. Sci. Comput., 43 (2021), pp. A1583–A1606, <https://doi.org/10.1137/20M1346225>.
- [26] J. QUERALES AND P. VENEGAS, *Mixed approximation of the axisymmetric acoustic eigenvalue problem*, Comput. Math. Appl., 108 (2022), pp. 1–11, <https://doi.org/10.1016/j.camwa.2021.12.013>.